

## MS No.: acp-2019-123

**Title:** *Exploiting multi-wavelength aerosol absorption coefficients in a multi-time resolution source apportionment study to retrieve source-dependent absorption parameters*

Authors: Alice C. Forello et al.

### Response to Reviewers

In addition to reviewers, the authors acknowledge very much the co-Editor for his suggestions. Comments from Referee #1 were also taken into account in the final version of the paper. The text was carefully checked and revised.

#### **Co-Editor Decision: Publish subject to minor revisions (review by editor) (03 Aug 2019)**

Comments to the Author:

Dear authors, Thank you very much for your revised manuscript.

The reviewer and I are generally satisfied with your changes. However, there are still many language and grammar issues in the current version. Therefore, the manuscript needs another thorough editorial read (preferable by a native speaker). Although it is not the work of the editor, I marked a few issues below (but not all of them due to limitations in time).

In addition, there are some other minor content issues which need clarification or improvement.

- Line 22: It should be “resolutions”.
- Line 28: Please remove the ‘...’ (you already say ‘e.g.’ at the beginning of the parenthesis).
- Line 32: Add ‘the’ before ‘atmosphere’.
- Line 34 and 36: Alpha and MAC are already defined in Line 19 and 20.
- Line 38: Suggest to move ‘approach’ behind ‘here presented’.
- Line 46: Suggest to replace ‘At the state of the art’ with ‘Currently’ or ‘As the state of the art’.
- Line 49: ‘proved’ -> ‘proven’. There should probably be a comma after ‘In the late 1990s’.
- Line 64: The variable of the absorption coefficient was already defined in line 58. Please add ‘to be’ before ‘proportional’.
- Line 76, line 81 and later: The word ‘source apportionment optical models’ sounds like a weird construct that is probably not correct. Strictly speaking, it is a model dealing with source apportionment and not with optics. Could you maybe rephrase it as e.g. “Source apportionment models based on optical measurements” or “Source apportionment models using optical measurements as input”?
- Line 82: ‘fuels’ -> ‘fuel’
- Line 84: Add ‘the’ before ‘atmosphere’.
- Line 85: ‘need a priori assumption about alpha values’ -> ‘need a priori assumptions on the alpha values’

- Line 94: This sentence is very long and hard to read. In addition, I would replace 'In the frame' by 'In the framework'.
- Line 95: Also this sentence is difficult to understand. I guess you want to say "Instead of using alpha as an a priori input, this approach even allows to retrieve alpha as a source-dependent value."?
- Line 102 (and throughout the manuscript): The word 'that' should not be preceded by a comma.
- Line 103: Please remove the '...'
- Line 104: Alpha has already been introduced many times before.
- Paragraph starting in line 106: This paragraph is a bit confusing and I suggest to rephrase it.
- Line 121: 'in activity' -> 'active'
- Line 178: 'Jülich Forschungszentrum' -> 'Forschungszentrum Jülich'
- The citation of 'Valentini et al.' is not an accepted or peer-reviewed publication and as such should be avoided as reference. I suggest to remove these sentences. It is sufficient that the comparison of the instrument is mentioned in the reply to the reviewers.
- Line 248 and 263: Add 'such' before 'as'.
- Line 265: What do you mean with under-weighed? Less weighed? How?
- Line 297: Suggest to replace 'Opposite' with 'In contrary'.
- Line 304: Add 'the' before 'factor'.
- Line 310: Alpha has been defined already many times before.
- Figure 1: Please add proper y-axis labels (e.g. 'Concentration' or 'Concentration Fe').
- Figure 2: Please add y-axis labels to the unit.
- Line 346: I suggest to add 'the' or 'a' before 'multi-time resolution model'
- Figure 3: It would be helpful to the reader if you describe 'F' and 'EVF' once more in the caption.
- Line 446: The reference to figure S3 is missing in this paragraph.
- Figure 4: As in the right axis, please also add the word 'concentration' or 'conc.' to the y-axis label in the left axis.
- Figure 5: The number on the y-axis for the biomass burning component are somehow wrong. Please check. The font size of the axis numbers is very small (it should be similar to the caption font size).
- Line 511: Alpha was already defined several times before.
- Line 539: Suggest to put a hyphen between alpha and value.
- Line 560: 'At' -> 'For' and add a comma after 'nm'.
- Line 561: Suggest to change it to 'report a MAC value of ...'.
- Line 581: Suggest to add a 'the' or 'a' before 'Multilinear'.
- Line 604: Remove the word 'works'.
- Figure S2: What does "scaled residuals" mean? Normalized by the mean/median? Please clarify in the caption. The y- and x-axis are also missing their proper labels and units.

- Figure S2: Suggest to also mention the year.

Please also consider and reply to the comments by reviewer #1.

*Answer: all comments and changes were implemented in the final version of the paper*

## **REFEREE #1**

The authors have responded well to the many points raised in the initial reviews. In particular, the inclusion of far more detail on the methods, and justifications for some of the procedures and assumptions are very welcome. There remain just a few minor points which could be improved.

(a) Lines 512-516 – the wording here is a little confusing. It seems to imply that the Delta-C method is not based on a 2-source hypothesis, whereas clearly it is. It may not have been the intention of the authors to imply this, but to refer to the Delta-C parameter as an input variable in receptor models. Some clarification would be beneficial.

*Answer: the sentence has been changed as follows “Another literature approach used Delta-C as an input variable together with chemical aerosol components in source apportionment models and was very effective in separating traffic (especially diesel) emissions from biomass combustion emissions (Wang et al., 2011, 2012).”*

(b) When discussing the factor associated with sulphate, the authors seek to explain the presence of EC within this factor in relation to the optical absorption, lines 497-501. It is worth bearing in mind that many receptor modelling studies have shown some presence of EC and trace elements in a secondary sulphate factor. This is most probably explicable by the fact that both EC and trace metals are emitted by many sources which also emit sulphur dioxide, for example, fuel oil combustion. Subsequent conversion of sulphur dioxide to sulphate will tend to lead to sulphate condensation on the primary emitted particles, hence leading to a more complex composition for this factor.

*Answer: the sentence has been changed as follows “Opposite to sulphates, EC has a primary origin; however, its presence with a very similar percentage (4-5 %) in a sulphate chemical profile was previously pointed out in Milan, indicating a more complex mixing between primary and secondary sources (Amato et al., 2016) e.g. with sulphate condensation on primary emitted particles. The sulphate factor accounted for 21 % of the PM10 mass.”*

(c) It is stated that during the monitoring campaign no significant contribution from mineral dust was observed (lines 549-550). This is expressed in the context of aerosol absorption. However, lines 505 to 508 attribute absorption by resuspended dust to the likely presence of iron minerals. If the term mineral dust is taken to refer to crustal materials and other largely inorganic particles such as those from construction works, then there is ample evidence of the presence of mineral dusts. The statement that there was no significant contribution from mineral dust may have been meant to refer to sources of pure crustal dust such as Saharan dust emissions, but greater clarity is needed here as the text currently appears contradictory.

*Answer: the sentence has been changed as follows “During our monitoring campaign, no contribution from Saharan dust was observed; opposite, biomass burning was proven to be an*

*important source so that BrC was certainly a significant contributor (Fuzzi et al., 2015) as also suggested by  $\alpha_{BB} = 1.83$  in the biomass burning factor.”*

**REFEREE #2**

Paper accepted as is.

# 1 Exploiting multi-wavelength aerosol absorption coefficients in a 2 multi-time resolution source apportionment study to retrieve 3 source-dependent absorption parameters

4 Alice C. Forello<sup>1</sup>, Vera Bernardoni<sup>1</sup>, Giulia Calzolai<sup>2</sup>, Franco Lucarelli<sup>2</sup>, Dario Massabò<sup>3</sup>, Silvia  
5 Nava<sup>2</sup>, Rosaria E. Pileci<sup>1,a</sup>, Paolo Prati<sup>3</sup>, Sara Valentini<sup>1</sup>, Gianluigi Valli<sup>1</sup>, Roberta Vecchi<sup>1,\*</sup>

6 <sup>1</sup>Department of Physics, Università degli Studi di Milano and National Institute of Nuclear Physics INFN-Milan, via  
7 Celoria 16, Milan, 20133, Italy

8 <sup>2</sup>Department of Physics and Astronomy, Università di Firenze and National Institute of Nuclear Physics INFN-Florence,  
9 via G. Sansone 1, Sesto Fiorentino, 50019, Italy

10 <sup>3</sup>Department of Physics, Università degli Studi di Genova and National Institute of Nuclear Physics INFN- Genoa, via  
11 Dodecaneso 33, Genoa, 16146, Italy

12 <sup>a</sup>now at: Laboratory of Atmospheric Chemistry (LAC), Paul Scherrer Institut (PSI), Forschungsstrasse 111, Villigen,  
13 5232, Switzerland

14

15 \*Correspondence to: Roberta Vecchi (roberta.vecchi@unimi.it)

16

17 **Abstract.** In this paper, a new methodology coupling aerosol optical and chemical parameters in the same source  
18 apportionment study is reported. In addition to results on sources ~~assessment~~contribution, this approach ~~gives~~  
19 ~~relevant~~provides information such as estimates for the atmospheric Absorption Ångström Exponent ( $\alpha$ ) of the sources  
20 and Mass Absorption Cross section (MAC) for fossil fuel emissions at different wavelengths.

21 A multi-time resolution source apportionment study using Multilinear Engine ME-2 was performed on a PM10 dataset  
22 with different time resolutions (24 hours, 12 hours, and 1 hour) collected during two different seasons in Milan (Italy) in  
23 2016. Samples were optically analysed by a home-made polar photometer to retrieve the aerosol absorption coefficient  
24  $b_{ap}$  (in  $Mm^{-1}$ ) at four wavelengths ( $\lambda=405$  nm, 532 nm, 635 nm and 780 nm) and were chemically characterised for  
25 elements, ions, levoglucosan, and carbonaceous components. The dataset joining chemically speciated and optical data  
26 was the input for ~~Time-resolved chemically speciated data were joined to  $b_{ap}$  multi-wavelength measurements and used~~  
27 ~~as input data in~~ the multi-time resolution receptor model; this approach was proven to strengthen the identification of  
28 sources thus being particularly useful when important chemical markers (e.g. levoglucosan, elemental carbon, ~~...~~) are not

29 available. The final solution consisted in 8 factors (nitrate, sulphate, resuspended dust, biomass burning, construction  
30 works, traffic, industry, aged sea salt); the implemented constraints led to a better physical description of factors and the  
31 bootstrap analysis supported the goodness of the solution. As for  $b_{ap}$  apportionment, consistently to what expected, ~~the~~  
32 ~~two factors assigned to~~ biomass burning and traffic were the main contributors to aerosol absorption in the atmosphere.  
33 A relevant feature of the approach proposed in this work is the possibility of retrieving many other information about  
34 optical parameters; for example, opposite to the more traditional approach used by optical source apportionment models,  
35 here we obtained the source-dependent atmospheric  $\alpha$  value ~~Absorption Angström Exponent ( $\alpha$ ) of the sources ( $\alpha$  biomass~~  
36 ~~burning = 1.83 and  $\alpha$  fossil fuels = 0.80)~~, without any a priori assumption ( $\alpha$  biomass burning = 1.83 and  $\alpha$  fossil fuels =  
37 0.80). In addition, ~~an estimate for the~~ MAC estimated ~~Mass Absorption Cross section (MAC)~~ for fossil fuel emissions ~~at~~  
38 ~~four wavelengths~~ was ~~obtained and found to be~~ consistent with literature ~~range values~~.  
39 It is worth noting that the ~~approach~~ here presented approach can be also applied using ~~widespread more common~~ receptor  
40 models (e.g. EPA PMF instead of multi-time resolution ME-2) if the dataset comprises variables with the same time  
41 resolution as well as optical data retrieved by ~~commercial~~ widespread instrumentation (e.g. an Aethalometer instead of  
42 home-made instrumentation).

43

## 44 1. Introduction

45 Atmospheric aerosol impacts both on local and global scale causing adverse health effects (Pope and Dockery, 2006),  
46 decreasing visibility (Watson, 2002), and influencing the climate (IPCC, 2013). To face these issues an accurate  
47 knowledge of aerosol emission sources is mandatory.

48 ~~At the state of the art~~ Currently, multivariate receptor models are considered a robust approach (Belis et al., 2015) to  
49 perform source apportionment studies and the Positive Matrix Factorization (PMF) (Paatero and Tapper, 1994) has  
50 become one of the most widely used receptor models (Hopke, 2016) in the aerosol community. In the late 1990s, the  
51 Multilinear Engine (ME-2) was developed and proved to be a very flexible algorithm to solve multilinear and quasi-  
52 multilinear problems (Paatero, 1999). The scripting feature of this algorithm allows the implementation of advanced  
53 receptor modelling approaches; one example is the multi-time resolution model (~~developed for the first time by~~ Zhou et  
54 al., (2004), which uses each experimental data in its original time schedule as model input. Source apportionment studies  
55 carried out by multi-time resolution model are still scarce in the literature (Zhou et al., 2004; Ogulei et al., 2005; Kuo et  
56 al., 2014; Liao et al., 2015; Crespi et al., 2016; Sofowote et al., 2018) although this methodology is very useful in  
57 measurement campaigns when ~~instrumentation instruments~~ with different time resolutions (minutes, hours or days) ~~is are~~  
58 available as high time resolution data can be exploited without averaging them over the longest sampling interval.

59 It is noteworthy that the combination of time-resolved chemically speciated data with the information obtained from  
60 instrumentation measuring aerosol optical properties at different wavelengths (e.g. the absorption coefficient  $b_{ap}$ ) is  
61 suggested as one of the future investigations of receptor modelling (Hopke, 2016); however, to the best of our knowledge,  
62 very few attempts in this direction have been done (e.g. Peré-Trepat et al., 2007; Xie et al., 2019). Wang et al. (2011,  
63 2012) ~~introduced~~ in a source apportionment study used the Delta-C (Delta-C = BC@370 nm – BC@880 nm from  
64 Aethalometer measurements) as an additional input variable and found that Delta-C was very useful in separating traffic  
65 from biomass burning source contributions.

66 The wavelength dependence of  ~~$b_{ap}$ , the aerosol absorption coefficient ( $b_{ap}$ )~~ can be empirically considered to be proportional  
67 to  $\lambda^{-\alpha}$ , where  $\alpha$  is the Absorption Ångström Exponent;  $\alpha$  depends on particles composition and size, and it is a useful  
68 parameter to gain information about particles type in atmosphere (see e.g. Yang et al., 2009). Among ~~PM aerosol~~  
69 components, black carbon (BC) is the main responsible for light absorption in atmosphere; in fact, it is considered the  
70 main ~~PM aerosol~~ contributor to global warming and the second most important anthropogenic contributor after CO<sub>2</sub> (Bond  
71 et al., 2013). Black carbon refers to a fraction of the carbonaceous aerosol ~~that shares characterised by~~ peculiar features  
72 ~~about as for~~ microstructure, morphology, thermal stability, solubility, and light absorption (Petzold et al., 2013); in  
73 particular, it is characterised by a wavelength-independent imaginary part of the refractive index over visible and near-  
74 visible regions. ~~In the last decade, experimental studies evidenced also the role of a~~ Another aerosol absorbing component  
75 ~~i.e. is~~ brown carbon (BrC), referred to as light-absorbing organic matter ~~of various origins~~ with increasing absorption  
76 towards lower wavelengths, especially in the UV region (Andreae and Gelencsér, 2006). BrC is an aerosol component  
77 that also affects the elemental vs. organic carbon correct separation when using thermal-optical methods as ~~recently~~  
78 outlined by Massabò et al. (2016).

79 Source apportionment ~~optical~~ models based only on multi-wavelength ~~measurements of~~  $b_{ap}$  data are available in the  
80 literature, i.e. the widespread Aethalometer model (Sandradewi et al., 2008a) and the more recent Multi-Wavelength  
81 Absorption Analyzer (MWAA) model (Massabò et al., 2015; Bernardoni et al., 2017b). Briefly, these models ~~allow to~~  
82 estimate the source contribution ~~of sources to~~ aerosol absorption ~~in atmosphere~~ exploiting their different dependence on  
83  $\lambda$  (i.e. different  $\alpha$ ). As a step forward, MWAA provides the  $b_{ap}$  apportionment in relation to both the sources (i.e. fossil  
84 fuel combustion and biomass burning) and the components (i.e. BC and BrC) and ~~gives also~~ provides an estimate for  $\alpha$   
85 of BrC. ~~Indeed,~~ ~~S~~ source apportionment ~~optical~~ models based on optical measurements data usually assume two  
86 contributors to  $b_{ap}$ , namely fossil fuels combustion and biomass burning (only few exceptions are present in the literature,  
87 e.g. Fialho et al., 2005). In most cases this assumption is well founded, except ~~in presence of when~~ episodic events ~~that~~  
88 ~~give giving~~ a not negligible contribution to aerosol absorption in the atmosphere occur, such as in presence of the transport  
89 ~~of~~ mineral dust from the Saharan desert (Fuzzi et al., 2015). Moreover, the above-mentioned models need a priori

90 assumptions ~~about~~ the  $\alpha$  values of the sources and wide ranges for  $\alpha$  are reported in the literature (e.g. Sandradewi et  
91 al., 2008a); this is the most critical step, since  $\alpha$  depends on the kind of fuel, burning conditions and aging processes in  
92 the atmosphere ~~and wide ranges for  $\alpha$  are reported in the literature (e.g. Sandradewi et al., 2008a)~~. Without accurate  
93 determination of source-specific atmospheric  $\alpha$  (for example exploiting the information derived from source  
94 apportionment using  $^{14}\text{C}$  measurements), the applicability of models based on optical ~~measurements data~~ is questionable  
95 (Bernardoni et al., 2017b; Massabò et al., 2015; Zotter et al., 2017). Moreover, the generally accepted assumption of  $\alpha=1$   
96 for fossil fuels and BC, ~~that is derived arising~~ from the theory of absorption ~~of by~~ spherical particles in the Rayleigh regime  
97 (Seinfeld and Pandis, 2006), might not always be valid ~~in the atmosphere due to aerosol aging processes for aged~~  
98 ~~atmospheric aerosol~~ (Liu et al., 2018).

99 In the framework of a source apportionment study based on multi-time resolution receptor modelling, ~~in this work~~ optical  
100 and chemical datasets were joined to explore the possibility of retrieving retrieve a multi- $\lambda$  apportionment of  $b_{\text{ap}}$  with no  
101 need of a-priori assumptions on the contributing sources. ~~Opposite, with this approach source-dependent  $\alpha$  values were~~  
102 ~~provided as output~~ Instead of using  $\alpha$  as an a priori input, this approach even allows to retrieve it as directly provided e  
103 source-dependent  $\alpha$  values. Moreover, the multi- $\lambda$  apportionment of  $b_{\text{ap}}$  in each source allowed to estimate MAC values  
104 at different wavelengths, exploiting the well-known relation  $\text{EBC} = b_{\text{ap}}(\lambda) / \text{MAC}(\lambda)$  (Bond and Bergstrom, 2006) ~~and~~  
105 ~~considering the apportioned concentrations of where~~ elemental carbon (EC) apportioned by the model was considered as  
106 a proxy for BC. The evaluation of atmospheric MAC values is also not trivial due to the possible presence of absorbing  
107 components different from BC (e.g. contribution from BrC, especially at lower wavelengths).

108 The original approach proposed in this work shows that coupling the chemical and optical information in a receptor  
109 modelling process is particularly advantageous because: (1) strengthens the source identification, that is particularly  
110 useful when relevant chemical tracers (e.g. levoglucosan, EC<sub>1</sub>, ~~EC<sub>2</sub>~~) are not available; (2) gives estimates for source-specific  
111 atmospheric  $\alpha$  Absorption Ångström Exponent ( $\alpha$ ) which are typically assumed a-priori in optical-source apportionment  
112 models based on optical measurements data; (3) ~~assesses provides~~ MAC values at different wavelengths for specific  
113 sources.

114 In this work, optical data were retrieved measured by a home-made multi-wavelength polar photometer and input data  
115 (chemical+optical) in the receptor model comprised variables acquired with different time resolutions. Anyway, it is  
116 worth noting that the here presented approach is of general interest as the same methodology could be applied to (1)  
117 datasets combining aerosol chemical and optical measurements data obtained by widespread instrumentation (e.g.  
118 Aethalometers for optical data); (2) variables with the same time resolution.

119 ~~It is also worth noting that the approach here presented is of general interest as (1) in this work optical data were retrieved~~  
120 ~~by a home-made multi-wavelength polar photometer but the same methodology could be applied to datasets combining~~  
121 ~~aerosol chemical and optical data obtained by widespread instrumentation (e.g. Aethalometers for optical data); (2) input~~  
122 ~~data to the receptor model not necessarily should comprise variables acquired with different time resolution as we did~~  
123 ~~here.~~

124

## 125 **2. Material and methods**

### 126 *2.1 Site description and aerosol sampling*

127 Two measurement campaigns were performed during summertime (June-July) and wintertime (November-December)  
128 2016 in Milan (Italy). Milan is the largest city (more than 1 million inhabitants, doubled by commuters everyday) of the  
129 Po Valley, a very well-known hot-spot pollution area in Europe due to both large emissions from a variety of sources (i.e.  
130 traffic, industry, domestic heating, energy production plants, and agriculture) and low atmospheric dispersion conditions  
131 (e.g. Vecchi et al., 2007 and 2019; Perrone et al., 2012; Bigi and Ghermandi, 2014; Perrino et al., 2014).

132 The sampling site is representative of the urban background and it is situated at about 10 meters above the ground, on the  
133 roof of the Physics Department of the University of Milan, less than 4 km far from the city centre (Vecchi et al., 2009).

134 It is important to note that during the sampling campaigns, a large building site was ~~in activity~~ active next to the monitoring  
135 station.

136 Aerosol sampling was carried out using instrumentation with different time ~~resolutions~~. Low time resolution PM10 data,  
137 with a sampling duration of 24 and 12 hours during summertime (20 June-22 July 2016) and wintertime (21 November-  
138 22 December 2016), respectively, were collected in parallel on PTFE (Whatman, 47 mm diameter) and pre-fired (700 °C,  
139 1 hour) quartz-fibre (Pall, 2500QAO-UP, 47 mm diameter) filters. Low volume samplers with EPA PM10 inlet operating  
140 at 1 m<sup>3</sup> h<sup>-1</sup> were used. High time resolution data were collected during shorter periods (11 July-18 July and 21 November-  
141 28 November 2016) by a streaker sampler (D'Alessandro et al., 2003). Shortly, the streaker sampler collects the fine and  
142 coarse PM fractions (particles with aerodynamic diameter  $d_{ac} < 2.5 \mu\text{m}$ , and  $2.5 < d_{ac} < 10 \mu\text{m}$ , respectively) with hourly  
143 resolution. Particles with  $d_{ac} > 10 \mu\text{m}$  impact on the first stage and are discarded; the coarse fraction deposits on the second  
144 stage, consisting of a Kapton foil; finally, the fine fraction is collected on a polycarbonate filter. The two collecting  
145 supports are kept in rotation with an angular speed of about 1.8° h<sup>-1</sup> to produce a circular continuous deposit on both  
146 stages.

147 Meteorological data were available at a monitoring station belonging to the regional environmental agency (ARPA  
148 Lombardia) which is less than 1 km far away.

149

150 2.2 PM mass concentration and chemical characterisation

151 In this Section, chemical analyses performed on samples are summarised. As ~~measured~~ concentration detected in each  
152 sample was characterised by its own uncertainty, only ranges for experimental uncertainties and minimum detection limits  
153 (MDLs) for every set of variables are reported.

154 PM<sub>10</sub> mass concentration was determined on PTFE filters by gravimetric technique. Weighing was performed by an  
155 analytical balance (Mettler, model UMT5, 1 µg sensitivity) after a 24 hours conditioning period in an air-controlled room  
156 as for temperature ( $20 \pm 1$  °C) and relative humidity ( $50 \pm 3$  %) (Vecchi et al., 2004).

157 These filters were then analysed by Energy Dispersive X-Ray Fluorescence (ED-XRF) analysis to obtain the elemental  
158 composition (details on the procedure can be found in Vecchi et al., 2004). For most elements and samples, concentrations  
159 were characterised by relative uncertainties in the range 7-20 % (higher uncertainties for elements with concentrations  
160 next to MDLs) and minimum detection limits of 0.9-30 ng m<sup>-3</sup> with the above mentioned sampling conditions.

161 For each quartz-fibre filter, one punch (1.5 cm<sup>2</sup>) was extracted by sonication (1 h) using 5 ml ultrapure Milli-Q water and  
162 ~~; this extract was analysed to measure both~~ levoglucosan and inorganic anions concentrations were quantified.

163 Levoglucosan concentration was determined by High-Performance Anion Exchange Chromatography coupled with  
164 Pulsed Amperometric Detection (HPAEC-PAD) (Piazzalunga et al., 2010) only in winter samples. Indeed, as already  
165 pointed out by other studies at the same sampling site (Bernardoni et al., 2011) and ~~as~~ routinely ~~measured~~ assessed at  
166 monitoring stations in Milan by the Regional Environmental Agency (private communication), levoglucosan  
167 concentrations during summertime are lower than the MDLs ~~of the technique~~ (i.e. about 6 ng m<sup>-3</sup>), due to both lower  
168 emissions (no influence of residential heating and negligible impact from other sources) and higher OH levels in the  
169 atmosphere depleting molecular markers concentrations (Robinson et al., 2006; Hennigan et al., 2010). Uncertainties on  
170 levoglucosan concentration were about 11 %. The measurement quantification of main water-soluble inorganic anions  
171 (SO<sub>4</sub><sup>2-</sup> and NO<sub>3</sub><sup>-</sup>) was performed by Ion Chromatography (IC); ~~these data had~~ MDLs ~~were of~~ 25 and 50 ng m<sup>-3</sup> with  
172 summertime and wintertime sampling conditions, respectively, and uncertainties ~~of~~ were about 10 %. Unfortunately, due  
173 to technical problems no data on ammonium were available. Details on the analytical procedure for IC analysis are  
174 reported in Piazzalunga et al. (2013).

175 Another punch (1.0 cm<sup>2</sup>) of each quartz-fibre filter was analysed by Thermal Optical Transmittance analysis (TOT, Sunset  
176 Inc., NIOSH-870 protocol) (Piazzalunga et al., 2011) in order to assess organic and elemental carbon (OC and EC)  
177 concentrations. MDLs ~~were~~ were 75 and 150 ng m<sup>-3</sup> with summertime and wintertime sampling conditions, respectively,  
178 and uncertainties were in the range 10-15 %.

179 Hourly elemental composition was assessed by Particle Induced X-ray Emission (PIXE) technique, using a properly  
180 collimated proton beam and scanning the deposits in steps corresponding to 1-hour aerosol deposit (details in Calzolari et

181 al., 2015). ~~As low time resolution PM10 samples were also available~~~~In this work~~, fine and coarse elemental concentrations  
182 determined by PIXE analysis were added up to obtain PM10 concentrations with hourly resolution ~~as low time resolution~~  
183 ~~PM10 samples were also available~~. PM10 hourly concentrations ~~of~~for most elements and samples were characterised by  
184 relative uncertainties in the range 10-30 % (higher uncertainties for elements near MDLs) and MDLs ranged from a  
185 minimum of 0.1 to a maximum of 15 ng m<sup>-3</sup> (higher MDLs typically detected for Z<20 elements).

186

### 187 2.3 Aerosol light-absorption coefficient measurements

188 The aerosol absorption coefficient ( $b_{ap}$ ) at the 4 wavelengths  $\lambda = 405, 532, 635$  and 780 nm was measured on both low  
189 and high time resolution samples with the home-made polar photometer PP\_UniMI (Vecchi et al., 2014; Bernardoni et  
190 al., 2017c). ~~Results on  $b_{ap}$  obtained by this custom photometer resulted in very good agreement against multi-angle~~  
191 ~~absorption photometer (MAAP) data at 635 nm (Vecchi et al., 2014; Bernardoni et al., 2017c). More recently, in the frame~~  
192 ~~of a collaboration with the Jülich Forschungszentrum (Germany), the Absorption Ångström Exponents retrieved by~~  
193 ~~extinction minus scattering measurements were compared at two wavelengths (630 nm and 450 nm) with the one obtained~~  
194 ~~by PP\_UniMI data for laboratory generated aerosols. The agreement with Cabot soot was in general very good as for~~  
195 ~~both  $b_{ap}$  at two wavelengths and Absorption Ångström Exponent estimates, i.e. comparability within one standard~~  
196 ~~deviation (data not yet published, preliminary results reported in Valentini et al., 2019).~~

197 Low time resolution optical measurements taken into account were those performed on PTFE filters since their physical  
198 characteristics can be considered more similar to polycarbonate filters used by the streaker sampler. Moreover, previous  
199 works reported a bias on  $b_{ap}$  measured by instrumentation using fibre filters (e.g. Cappa et al., 2008; Lack et al., 2008;  
200 Davies et al., 2019; and references therein), ~~Vecchi et al. (2014) found that  $b_{ap}$  at 635 nm was 40% higher when~~  
201 ~~measured on quartz-fibre filter compared to parallel samples collected on PTFE. quantified in about 40 % the effect~~  
202 ~~caused in  $b_{ap}$  values (assessed at 635 nm) by sampling. This effect was ascribed to sampling artefacts due to organics in~~  
203 ~~aerosol samples collected in Milan when comparing aerosol samples collected in parallel quartz fibre and PTFE filters.~~

204 ~~As f~~For high time resolution samples,  $b_{ap}$  was measured only in the fine fraction collected on polycarbonate filters, since  
205 absorption ~~from of~~ the Kapton foil on which the coarse fraction was collected did not allow  $b_{ap}$  assessment. Anyway,  $b_{ap}$   
206 values in PM2.5 and PM10 were expected to be fairly comparable, as ~~most of the contribution to~~ aerosol absorption in  
207 atmosphere is ~~typically given by~~ mostly due to particles in the fine fraction at heavily polluted urban sites like Milan. To  
208 verify this assumption, high time resolution  $b_{ap}$  data in PM2.5 were averaged ~~on over~~ the time scale of low time resolution  
209  $b_{ap}$  in PM10 and compared; the agreement was good, for comparison. ~~They turned out to be in good agreement,~~ between  
210 11 % and 13 % depending on the  $\lambda$ , except for  $b_{ap}$  at  $\lambda=405$  nm that showed a higher difference (27 %) but with most data  
211 (83 %) within experimental uncertainties. To take into account ~~for~~ this difference,  $b_{ap}$  data at  $\lambda=405$  nm were homogenised

212 before ~~their insertion into~~ using them in the model, following the criterion used for chemical species (for further detail  
213 about homogenisation procedure, see Sect. 2.4 and Sect. 2.5).  
214 Uncertainties on  $b_{ap}$  were ~~estimated as~~ quantified in 15 % and MDL was in the range 1-10  $Mm^{-1}$  depending on sampling  
215 duration and wavelength as already reported in ~~our previous works~~ (Vecchi et al. (2014) and Bernardoni et al. (2017c).  
216 ~~Experimental uncertainties and MDL of optical absorption data were used as a starting point to estimate the uncertainties~~  
217 ~~introduced in the model.~~ Pre-treatment procedure for experimental uncertainties and MDL ~~these data~~ was the same used  
218 for chemical variables in order to create suitable input matrices required by the multi-time resolution model (see also Sect.  
219 2.5). Optical system stability was checked during the measurement session, evaluating the reproducibility of the  
220 measurement on a blank test filter. Laser stability was also checked at least twice a day and the recorded intensities were  
221 used to normalise blank and sampled filters analysis.

222

#### 223 2.4 Model description

224 Multivariate receptor models (Henry, 1997) are among the most widespread and robust approaches used to carry out  
225 source apportionment studies for atmospheric aerosol (Belis et al., 2014 and 2015). In particular, the Positive Matrix  
226 Factorization PMF2 (Paatero and Tapper, 1994; Paatero, 1997) had been extensively used in the literature and, afterwards,  
227 the Multilinear Engine ME\_2 (Paatero, 1999 and 2000) introduced the possibility of solving all kinds of multilinear and  
228 quasi-multilinear problems. The fundamental principle of these modelling approaches is the mass conservation between  
229 the emission source and the receptor site; using the information carried by aerosol chemical composition assessed ~~on a~~  
230 ~~number of in~~ samples collected at the receptor site, a mass balance analysis can be performed to identify the factors  
231 influencing aerosol mass concentrations (Hopke, 2016). Factors can be subsequently interpreted as the main sources  
232 impacting the site, ~~exploiting through the~~ knowledge about ~~the most relevant~~ major sources in the investigated area and  
233 the ~~adoption-exploitation~~ of chemical fingerprints available from previous literature works (Belis et al., 2014). Referring  
234 to the input data as matrix X (matrix elements  $x_{ij}$ ), the chemical profile of the factors as matrix F (matrix elements  $f_{kj}$ ),  
235 and the time contribution of the factors as matrix G (matrix elements  $g_{ik}$ ), the main equation of a bilinear problem can be  
236 written as follows:

$$237 \quad x_{ij} = \sum_{k=1}^P g_{ik} f_{kj} + e_{ij} \quad (1)$$

238 where the indices i, j, and k indicate the sample, the species, and the factor, respectively; P is the number of factors and  
239 the matrix E (matrix elements  $e_{ij}$ ) is composed by the residuals, i.e. the difference between measured and modelled values.  
240 In this way, a system of NxM equations is established, where N is the number of samples and M is the number of species.  
241 The solution of the problem is computed minimising the object function Q defined as:

242 
$$Q = \sum_{i=1}^N \sum_{j=1}^M \left( \frac{e_{ij}}{\sigma_{ij}} \right)^2 \quad (2)$$

243 where  $\sigma_{ij}$  are the uncertainties related to the input data.

244 The multi-time resolution receptor model was developed in order to use each data value in its original time schedule,  
 245 without averaging the high time resolution data or interpolating the low time resolution data (Zhou et al., 2004; Ogulei et  
 246 al., 2005). The main Eq. (1) is consequently modified as below:

247 
$$x_{sj} = \frac{1}{t_{s2} - t_{s1} + 1} \sum_{k=1}^P f_{kj} \sum_{i=t_{s1}}^{t_{s2}} g_{ik} \eta_{jm} + e_{sj} \quad (3)$$

248 where the indices s, j, and k indicate the sample, the species and the factor respectively; P is the number of factors;  $t_{s1}$  and  
 249  $t_{s2}$  are the starting and ending time for the s-th sample in time units (i.e. the shortest sampling interval, that is 1 hour for  
 250 the dataset used here) and i represents one of the time units of the s-th sample.  $\eta_{jm}$  are adjustment factors for chemical  
 251 species replicated with different time resolution and measured with different analytical methods (represented by the  
 252 subscript m).

253 If  $\eta$  is close to unity, species concentration measured by different analytical approaches can be considered in good  
 254 agreement; non-replicated species have adjustment factors set to unity by default. In this work, the adjustment factors  
 255 were always set to unity in the model; to take into account the use of ~~different~~ two types of aerosol samplers (i.e. low  
 256 volume sampler with EPA inlet and streaker sampler) and different analytical techniques to obtain the elemental  
 257 composition (i.e. ED-XRF and PIXE), concentrations of replicated species with ~~different multiple time resolution time~~  
 258 resolutions were homogenised before inserting them into the input matrix X, as will be explained in Sect. 2.5. Applying  
 259 ~~†This data treatment procedure, it is possible to avoid to~~ avoids the consistency check ~~between if the~~  $\eta$  values calculated  
 260 by the model ~~are consistent with~~ and differences in experimental data characterised by high and low time resolution.  
 261 Otherwise, this step should always be performed after running the model.

262 In the multi-time resolution model ~~the following~~ regularisation equation is introduced to take into account that, since  
 263 some sources could contain few or no species measured with high time resolution:

264 
$$g_{(i+1)k} - g_{ik} = 0 + \varepsilon_i \quad (4)$$

265 where  $\varepsilon_i$  represent the residuals.

266 As already pointed out by Ogulei et al. (2005), a weighing parameter for low resolution species might be necessary; in  
 267 this study, it was implemented in the equations and set at 0.5 for strong species (not applied to weaker species such as  
 268 Na, Mg, and Cr, see Sect. 2.5) in 24-h or 12-h samples.

269 Equations (3) and (4) are solved using the Multilinear Engine (ME) program (Paatero, 1999). In Eq. (2), the object  
270 function Q takes into account residuals from the main Eq. (3) and from the auxiliary equations (regularisation Eq. (4),  
271 normalisation equation, pulling equations, and constraints).

272 In this work, the multi-time resolution model implemented by Crespi et al. (2016) was used; therefore, constraints were  
273 inserted in the model and the bootstrap analysis was also performed to evaluate the robustness of the final solution.

274

### 275 *2.5 Input data*

276 As already mentioned in Sect. 2.4, instead of using adjustment factors in the model (all set equal to one), concentrations  
277 of replicated species with different ~~time resolution~~ time resolutions were pre-homogenised and then inserted into the input  
278 matrix X. Concentration data with longer sampling interval (24 and 12 hours in this work) were considered as benchmark,  
279 since analytical techniques usually show a better accuracy on concentration values far from MDLs (i.e. samples collected  
280 on longer time intervals) (Zhou et al., 2004; Ogulei et al., 2005).

281 Variables were then classified as weak and strong according to the signal-to-noise ratio (S/N) criterion (Paatero, 2015).

282 For hourly data only strong variables ( $S/N \geq 1.2$ ) were considered; for low time resolution data also weak ~~or~~ variables  
283 such as Na, Mg and Cr (with S/N equal to about 0.8), that resulted strong variables in hourly samples, were also included  
284 although ~~under weighed (i.e. with~~ associated uncertainties comparable to concentration values) in order to avoid the  
285 exclusion of too many data. Indeed, excluding these low time resolution variables from the analysis gave rise to artificial  
286 high values in the time contribution matrix for sources traced by these species (in this case it was particularly important an  
287 issue for aged sea salt traced by Na and Mg, see Sect. 3.2); this oddity was already reported by Zhou et al. (2004).

288 Every measured variable in each sample is characterised by its own uncertainty; ranges of experimental uncertainties and  
289 MDLs are reported in Sect. 2.2 and 2.3 for chemical and optical analyses, respectively. Variables with more than 20 %  
290 of the concentration data below MDL values were omitted from the analysis (Ogulei et al., 2005). Uncertainties, missing  
291 values and data below minimum detection limits were pre-treated according to ~~The procedure described in~~ Polissar et al.  
292 (1998) ~~was followed to treat uncertainties and below MDL data, starting from experimental uncertainties and MDLs.~~

293 In general, missing concentration values were estimated by linear interpolation of the measured data and their uncertainties  
294 were assumed as three times this estimated value (Zhou et al., 2004; Ogulei et al., 2005). As for summertime levoglucosan  
295 data (~~not available~~ always below MDLs), the approach was to include them as below MDL data and not as missing data  
296 following Zhou et al. (2004), who underlined that the multi-time resolution model is more sensitive to missing values  
297 than the original PMF model. In order to avoid double counting, in this study S was chosen as input variable instead of  
298  $SO_4^{2-}$  as it was determined on both low time and high time resolution samples (by XRF and PIXE analysis, respectively,  
299 see Calzolari et al., 2008). However, elemental  $SO_4^{2-}$  and S concentrations showed a high correlation (correlation

300 coefficient  $R=0.98$ ) and the Deming regression gave a slope of  $2.69 \pm 0.13$  (sulphate vs. sulphur) with an intercept of -  
301  $198 \pm 82 \text{ ng m}^{-3}$ , i.e. compatible with zero within 3 standard deviations. The slight difference (of the order of 10%)  
302 between the estimated slope and the  $\text{SO}_4^{2-}$ -to-S stoichiometric coefficient (i.e. 3) can be ascribed to either a small fraction  
303 of insoluble sulphate or to the use of different analytical techniques.

304 PM10 mass concentrations were included in the model with uncertainties set at four times their values (Kim et al., 2003).  
305 In the end, 22 low time resolution variables (PM10 mass, Na, Mg, Al, Si, S, K, Ca, Cr, Mn, Fe, Cu, Zn, Pb, EC, OC,  
306 levoglucosan,  $\text{NO}_3^-$ ,  $b_{\text{ap}} 405\text{nm}$ ,  $b_{\text{ap}} 532\text{nm}$ ,  $b_{\text{ap}} 635\text{nm}$ ,  $b_{\text{ap}} 780\text{nm}$ ) and 17 hourly variables (Na, Mg, Al, Si, S, K, Ca, Cr,  
307 Mn, Fe, Cu, Zn, Pb,  $b_{\text{ap}} 405\text{nm}$ ,  $b_{\text{ap}} 532\text{nm}$ ,  $b_{\text{ap}} 635\text{nm}$ ,  $b_{\text{ap}} 780\text{nm}$ ) were considered.

308 The input matrix X consisted in 386 samples and the total number of time units was 1117. The analysis was performed  
309 in the robust mode; lower limit for G contribution was set to -0.2 (Brown et al., 2015) and the error model  $\text{em}=-14$  was  
310 used for the main equation with  $C_1=$  input error,  $C_2= 0.0_2$  and  $C_3=0.1$  (Paatero, 2012) for both chemical and optical  
311 absorption data.

312 Sensitivity tests on the uncertainty of absorption data were performed starting from a minimum uncertainty of 10 %.  
313 Lower uncertainties were considered not physically meaningful from an experimental point of view. ME-2 analyses  
314 performed with 10 % uncertainty on absorption data gave very similar results to the base case solution presented in the  
315 Supplement (Figure S1 and Table S3), with no differences in mass apportionment and a maximum variation in the  
316 concentrations of chemical and optical profiles (matrix F) of 7 % when considering significant variables in each profile  
317 (i.e. EVF higher or near 0.30). ~~Opposite~~In contrary, considering an uncertainty of 20 % on absorption data, the solution  
318 significantly differed from ~~the base case one presented~~the one reported in the Supplement and showed less physical  
319 meaning (e.g. a couple of factors got mixed, an additional unique factor appeared giving a null mass contribution). ~~Indeed,~~  
320 ~~the factors assigned to resuspended dust and construction works got mixed, and a new unique factor (traced almost~~  
321 ~~exclusively by Pb) appeared, with mass contribution equal to zero.~~ Thus, the estimated relative uncertainty of 15 % was  
322 here considered appropriate for optical variables.

323 It is also noteworthy that ME-2/PMF analysis is not a-priori harmed by the use of joint matrices containing different units  
324 (see e.g. Paatero, 2018). Indeed, if different units are present in different columns of matrix X, the output data in the factor  
325 matrix G are pure numbers and elements in a column of the factor matrix F carry the same dimension and unit as the  
326 original data in matrix X. In addition, ~~as we did in this work,~~ the average total contribution to the mass of a specific source  
327 due to species in a certain factor in matrix F must be retrieved a-posteriori summing up only mass contributions by  
328 chemical components (i.e. excluding optical components in matrix F).

329 To the authors' knowledge, this ~~is was~~ the first time that the absorption coefficients ~~at~~ at different wavelengths ~~were~~ ~~was~~  
330 introduced in the multi-time resolution model jointly with chemical variables and used to more robustly identify the

331 sources; moreover, ~~this approach led to the assessment of source-dependent~~ ~~the optical information was also exploited to~~  
332 ~~retrieve additional information such as the  $\alpha$  values~~ Absorption Ångström Exponent ( $\alpha$ ) ~~of the sources~~ and MAC values  
333 in an original way.

334

### 335 3. Results and discussion

#### 336 3.1 Concentration values

337 In Table S1 (Supplement) basic statistics on mass and chemical species concentrations at different time resolutions are  
338 given.

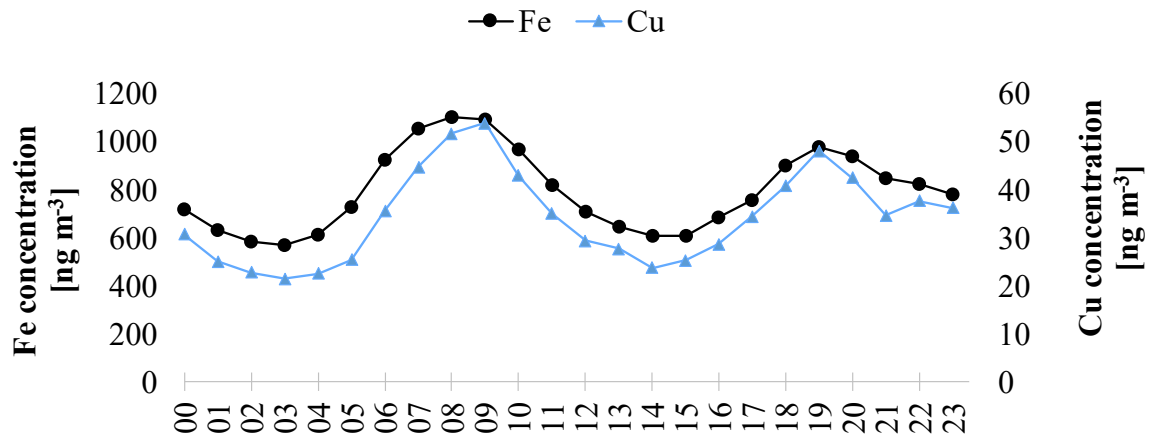
339 Most variables showed higher mean and median concentrations during the winter campaign, when atmospheric stability  
340 conditions influenced the monitoring site; exceptions were Al, Si and Ca which had lower median concentrations (as  
341 detected in low time resolution samples). This was not unexpected as they are typical tracers of soil dust resuspension  
342 (Viana et al., 2008) that can be more relevant during summertime due to drier soil conditions and ~~higher~~ ~~stronger~~  
343 atmospheric turbulence. Moreover, the good correlation between these elements (Al vs Si:  $R^2=0.94$  and Ca vs Si:  $R^2=0.78$ )  
344 suggested their common origin.

345 Potassium ~~showed the clearest seasonal behaviour in concentration values~~ ~~was the element showing the most different~~  
346 ~~median concentrations in the two seasons; its median concentration in low time resolution samples was going from~~ 284  
347  $\text{ng m}^{-3}$  (10<sup>th</sup>-90<sup>th</sup> percentile: 151-344  $\text{ng m}^{-3}$ ) ~~and to~~ 660  $\text{ng m}^{-3}$  (10<sup>th</sup>-90<sup>th</sup> percentile: 349-982  $\text{ng m}^{-3}$ ) in summer and  
348 winter, respectively, in low time resolution samples. K is an ambiguous tracer, since it is emitted by a variety of sources  
349 ~~such as~~ among which there are crustal resuspension and biomass burning. In our dataset, wintertime K values showed a  
350 good correlation with levoglucosan concentrations ( $R^2=0.71$ ) suggesting ~~an~~ ~~the~~ impact of biomass burning as  
351 levoglucosan is a well-known tracer for biomass burning emissions in winter samples (Simoneit al., 1999). Also looking  
352 at K-to-Si ratio (~~the latter where Si was~~ taken as soil dust marker) significant seasonal differences came out; it was  $0.35 \pm$   
353  $0.15$  in high time resolution summer samples and  $2.0 \pm 2.2$  in winter ones, to be compared with the much more stable Al-  
354 to-Si ratio ~~for Al/Si~~ (i.e.  $0.26 \pm 0.04$  and  $0.28 \pm 0.09$  in summer and winter, respectively) indicating a soil-related origin.

355 Among the elements typically associated to anthropogenic sources, Fe and Cu showed a good correlation (e.g.  $R^2=0.72$   
356 on hourly resolution samples) as well as Cu and EC (Cu vs EC:  $R^2=0.84$ , on low time resolution data); ~~in~~ ~~addition~~, the  
357 diurnal pattern of Fe and Cu showed traffic rush-hours peaks (7-9 a.m. and around 19 p.m. as shown in Fig.1). These  
358 results were suggestive of a common source. ~~Indeed, in the literature~~ these aerosol chemical components are reported ~~in~~  
359 ~~the literature~~ as tracers for vehicular emissions (e.g. Viana et al., 2008; Thorpe and Harrison, 2008).

360

361



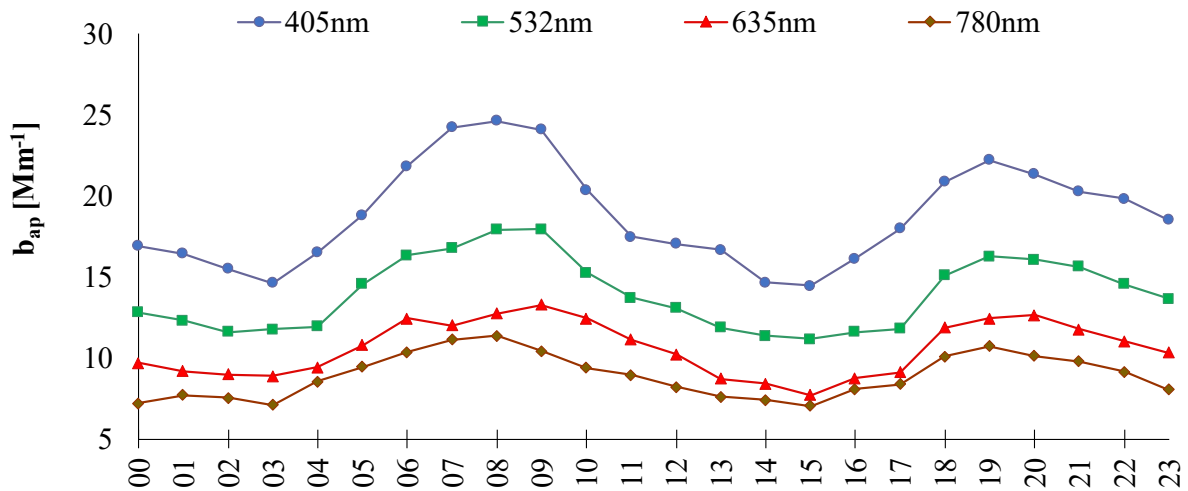
362

363 Figure 1: Diurnal profile of Fe and Cu concentrations (in ng m<sup>-3</sup>).

364

365 In Table S2 (Supplement) also basic statistics on  $b_{ap}$  values referred to low resolution samples collected on PTFE are  
366 reported. Diurnal mean temporal patterns for  $b_{ap}$  at different wavelengths (retrieved from hourly resolved data) are  
367 displayed in Fig. 2.

368



369

370 Figure 2: Diurnal profile of aerosol absorption coefficient ( $Mm^{-1}$ ) measured at different wavelengths.

371

372 3.2 Source apportionment with the multi-time resolution model

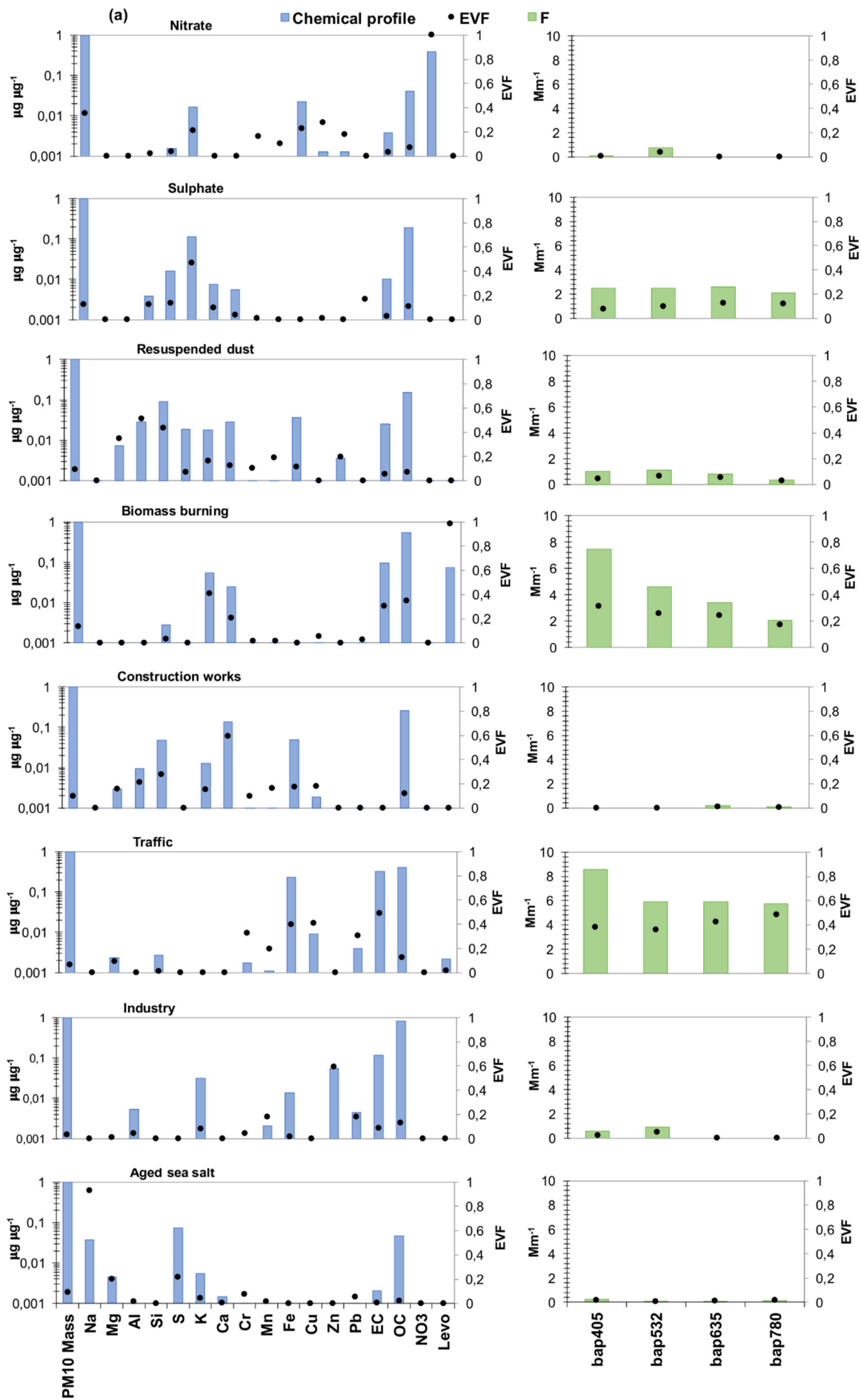
373 Different ~~solutions (from 5 to 10 factors)~~ ~~number of factors (5-10)~~ were explored; after 30 convergent runs, the 8-factor  
374 base-case solution corresponding to the lowest Q value (2086.88) was firstly selected (see Fig. S1 in the Supplement). It  
375 is important to ~~note~~note that the model was run using all variables (chemical + optical) as explained in Sect. 2.5. A  
376 lower or higher number of factors caused ambiguous chemical profiles and the physical interpretation ~~singled~~  
377 ~~outsuggested~~ clearly mixed sources for a lower number of factors or unique factors in case of more factors (i.e. Pb for 9  
378 factors); moreover, inconsistent mass closure was detected increasing the number of factors (e.g. the sum of species  
379 contribution was up to 25 % higher than the mass for the 10-factor solution). In the 8-factor base case solution, the mass  
380 was well reconstructed by the model ( $R^2=0.98$ ), with a slope of  $0.98 \pm 0.02$  and negligible intercept ( $=0.51 \pm 0.89 \mu\text{g m}^{-3}$ ).

382 The factor-to-source assignment ~~process~~ was based on both the Explained Variation for F matrix (EVF) values - which  
383 are typically higher for chemical tracers (Lee et al., 1999; Paatero, 2010) - and the physical consistence of factor chemical  
384 profiles. In the chosen solution, the not explained variation was lower than 0.25 for all variables. The uncertainty-scaled  
385 residuals (Norris et al., 2014) showed a random distribution of negative and positive values in the  $\pm 3$  range, with a  
386 Gaussian shape for most of the variables (Fig. S2 in the Supplement).

387 Using EVF and chemical profiles reported in Fig. S1(a), the 8 factors were tentatively assigned to ~~specific atmospheric~~  
388 ~~aerosol sources~~: nitrate, sulphate, resuspended dust, biomass burning, construction works, traffic, industry, and aged sea  
389 salt. In Table S3 (in the Supplement) absolute and relative average source contributions to PM10 mass are reported.

390 Although the above mentioned base-case solution was a satisfactory representation of the main sources active in the area  
391 (as reported in previous works, see e.g. Marcazzan et al., 2003; Vecchi et al., 2009 and 2018; Bernardoni et al., 2011 and  
392 2017a; Amato et al., 2016), the chemical profiles of some factors were improved exploring rotated solutions. The most  
393 relevant case was represented by aged sea-salt where typical diagnostic ratios such as Mg/Na and Ca/Na (in bulk sea  
394 water equal to 0.12 and 0.04, respectively, as reported e.g. in Seinfeld and Pandis, 2006) were not well reproduced in the  
395 base-case solution (~~in bulk sea water equal to 0.12 and 0.04, respectively, as reported e.g. in Seinfeld and Pandis, 2006~~)  
396 and the chemical profile ~~itself~~ was too much impacted by the presence of Fe compared to bulk sea water composition.  
397 Therefore, the above-mentioned diagnostic ratios were here used as constraints and Fe was maximally pulled down in the  
398 chemical profile. The effective increase in Q was of about 61 units ( $Q=2147$ ), with a percentage increase of about 3 %;  
399 as a rule of thumb, an increase in the Q value of a few tens is generally considered acceptable (Paatero and Hopke, 2009).  
400 It is noteworthy that the constrained solution led to an improvement in the chemical profile of the aged sea salt profiles  
401 was achieved and with negligible differences in all other relevant features of the solution (i.e. EVF, residuals, mass  
402 reconstruction, source apportionment) were found compared to the base-case solution ~~as for all other relevant features of~~

403 ~~the solution (i.e. EVF, residuals, mass reconstruction, source apportionment).~~ Therefore, the 8-factor constrained solution  
404 was considered the most physically reliable; results are presented in Table 1 and Fig. 3 and discussed in detail in the  
405 following.



407 Figure 3: (a) Chemical profiles of the 8-factor constrained solution ; (b)  $b_{ap}$  apportionment of the 8-factor constrained  
 408 solution. The blue bars represent the chemical profile (output of the matrix F normalised on mass), the green bars the  
 409 output values of the matrix F for the optical variables, and the black dots the EVF.

410

Factors	Summer [ $\mu\text{g m}^{-3}$ ]	Winter [ $\mu\text{g m}^{-3}$ ]	Total [ $\mu\text{g m}^{-3}$ ]
Nitrate	3.6 (15 %)	21.1 (44 %)	10.2 (31 %)
Sulphate	6.3 (26 %)	8.1 (17 %)	7.0 (21 %)
Resuspended dust	4.6 (19 %)	1.7 (4 %)	3.5 (11 %)
Biomass burning	0.32 (1 %)	8.3 (17 %)	3.3 (10 %)
Construction works	5.9 (24 %)	3.4 (7 %)	4.9 (15 %)
Traffic	1.4 (6 %)	2.2 (5 %)	1.7 (5 %)
Industry	0.86 (4 %)	1.2 (3 %)	1.0 (3 %)
Aged sea salt	1.4 (6 %)	1.8 (4 %)	1.6 (5 %)

411 Table 1: Absolute and relative average source contributions to PM10 mass in the 8-factor constrained solution.

412

413 The factor interpreted as nitrate fully accounted for the explained variation of  $\text{NO}_3^-$ . This factor contained a significant  
 414 fraction of nitrate in the chemical profile (39 %) and all nitrate was present only in this factor. This source was by large  
 415 the most significant one at the investigated site, explaining about 31 % of the PM10 mass over the whole campaign (a  
 416 similar estimate – 26 % - was reported by Amato et al. (2016) during the AIRUSE campaign in Milan in 2013) raising up  
 417 to 44 % during wintertime (comparable to 37 % reported by Vecchi et al. (2018)). Indeed, the Po valley is well-known  
 418 for experiencing very high nitrate concentrations during wintertime (Vecchi et al., 2018; and references therein) because  
 419 of large emissions of gaseous precursors related to urban and industrial activities, biomass burning used for residential  
 420 heating, high ammonia levels due to agricultural fields manure and ~~last but not the least~~ poor atmospheric dispersion  
 421 conditions.

422 The factor associated to sulphate ~~shows~~ showed EVF=0.47 for S and much lower EVF for all the other variables in the  
 423 factor. Considering the sulphur contribution ~~of S~~ in the chemical profile in terms of sulphate and ammonium sulphate,  
 424 the relative contribution of sulphur components in the profile ~~increases~~ increased from 11 % (S) up to 45 % (ammonium  
 425 sulphate). The latter is the main sulphur compound detected in the Po valley as reported in previous papers such as e.g.  
 426 Marcazzan et al. (2001) and was by far the highest contributor in the chemical profile. The other important contributor  
 427 was OC (19 %), whose impact on PM mass increased up to 30 % when reported as organic matter using 1.6 as the organic  
 428 carbon-to-organic matter conversion factor for this site (Vecchi et al., 2004). Due to the secondary origin of the aerosol  
 429 associated to this factor, it was not surprising to find also a significant OC contribution; indeed, aerosol chemical  
 430 composition in Milan is impacted by highly oxygenated components due to aging processes favoured by strong  
 431 atmospheric stability (Vecchi et al., 2018 and 2019). In this factor, EC contributed for about 1 %. Considering the total  
 432 EC concentration reconstructed by the model, the EC fraction related to the sulphate factor was about 6 %. Opposite to

433 sulphates, EC has a primary origin; however, its presence with a very similar percentage (4-5 %) in a sulphate chemical  
434 profile was previously pointed out in Milan, indicating a more complex mixing between primary and secondary sources  
435 (Amato et al., 2016) e.g. with sulphate condensation on primary emitted particles. -The sulphate factor accounted for 21  
436 % of the PM10 mass.

437 The factor identified as resuspended dust is mainly characterised by high ~~EVFs~~EVF and contributions coming from Al,  
438 Si and Mg, i.e. crustal elements. The Al/Si ratio is 0.31, very similar to the literature value for average crustal composition  
439 (Mason, 1966); the relatively high OC contribution ~~of OC~~in the chemical profile (15 %) ~~and together with~~ the presence  
440 of EC (about 2.6 %) is suggestive of, indicate that there is very likely a mixing with road dust (Thorpe and Harrison,  
441 2008). This source accounts for about 11 % of the PM10 mass.

442 The factor identified as biomass burning was characterised by high EVF for levoglucosan (0.98), a known tracer for this  
443 source as it is generated by cellulose pyrolysis; EVF higher than 0.3 were also found for K, OC, and EC. In the source  
444 chemical profile, OC contributed for 54 %, EC for 10 %, levoglucosan for 7 %, and K for 5 %. The average biomass  
445 burning contribution during this campaign was 10 % (up to 17 % in wintertime). Anticipating the discussion presented in  
446 detail in Sect. 3.3, it is worth ~~noticing~~noting that the second largest contribution to the aerosol absorption coefficient after  
447 traffic was detected in this factor.

448 The factor with high EVF (0.60) for Ca was associated to construction works, following literature works (e.g. Vecchi et  
449 al., 2009; Bernardoni et al., 2011; Dall'Osto, 2013; Crilley et al., 2017; Bernardoni et al., 2017a; and references therein).  
450 Major contributors to the chemical profile were Ca (13 %), OC (26 %), Fe, and Si (5 % each). This factor accounted on  
451 average for 15 % to PM10 mass. As already mentioned, during the campaign a not negligible contribution from this  
452 source was expected, due to the presence of a ~~construction~~building site nearby the monitoring location.

453 In the factor ~~here~~assigned to traffic (primary contribution), EVF larger than 0.3 characterised EC, Cu, Fe, Cr, and Pb.  
454 The highest relative mass contributions ~~in terms of mass~~in the chemical profile were given by OC (41 %), EC (32 %),  
455 Fe (23 %), and Cu (1 %). The lack of relevant crustal elements such as Ca and Al in the chemical profile, suggested a  
456 negligible impact of road dust in this factor. As reported above, at our sampling site the road dust contribution was very  
457 likely mixed to resuspended dust and further separation of these contributions was not possible. This traffic (primary)  
458 contribution over the whole dataset accounted for 5 % of the PM10 mass with a slightly lower absolute contribution in  
459 summer (see Table 1). This contribution is comparable to the percentage (7 %) reported by Amato et al. (2016) for exhaust  
460 traffic emissions but it is lower than our previous estimates (Bernardoni et al., 2011; Vecchi et al., 2018), i.e. 15 % in  
461 2006 in PM10 and 12 % in PM1 recorded in winter 2012. However, the current estimate seems to be still reasonable when  
462 considering the efforts done in latest years to reduce vehicles exhaust particle emissions and the fraction of secondary  
463 nitrate due to high nitrogen oxides and ammonia emissions in the region (INEMAR ARPA-Lombardia, 2018) which has

464 to be added to account for the overall traffic impact; ~~indeed, a significant traffic contribution due to nitrate should be~~  
465 ~~accounted for the relevant nitrogen oxides and ammonia emissions from agriculture in the region (INEMAR ARPA-~~  
466 ~~Lombardia, 2018).~~ Unfortunately, the non-linearity of the emission-to-ambient concentration levels relationship and the  
467 high uncertainties in emission inventories still prevent a robust estimate of this secondary contribution to total traffic  
468 exhaust emissions. As shown in Sect. 3.3, ~~it will be shown that~~ traffic is the largest contributor to aerosol absorption  
469 coefficient ~~thus strengthening, a result that reinforces~~ the interpretation of this factor as a traffic emission source.

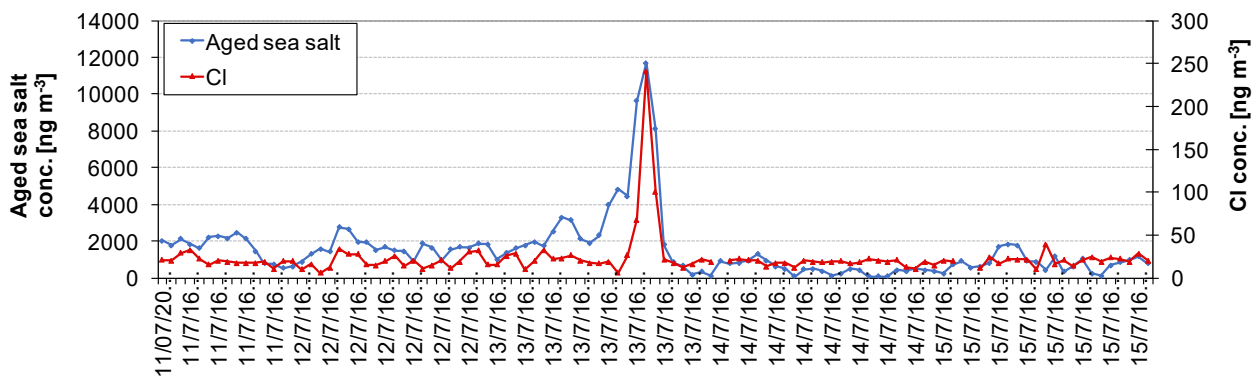
470 The industry factor showed high EVF for Zn (0.59) and the second highest EVF was related to Mn (0.13). Previous studies  
471 at the same sampling site identified these elements as tracers for industrial emissions (e.g. Vecchi et al., 2018; and  
472 references therein). The chemical profile resulted enriched by heavy metals and, after traffic, it was the profile with the  
473 highest share of Cr, Mn, Fe, Cu, Zn, and Pb (explaining about 8 % of the total PM<sub>10</sub> mass in the profile). The industry  
474 contribution was not very high in the urban area of Milan, accounting for 3 % on average.

475 The factor interpreted as aged sea salt was characterised by high EVF of Na (0.93) and this element was - as a matter of  
476 fact - present only in this factor chemical profile. To check the physical consistency of this assignment and considering  
477 that Milan is about 120 km away from the nearest sea coast, back-trajectories coloured by the aged sea salt concentration  
478 (in ng m<sup>-3</sup>) were calculated through the NOAA HYSPLIT trajectory model (Draxler and Hess, 1998; Stein et al., 2015;  
479 Rolph et al., 2017) and represented using the ~~R package Openair software~~ (Carslaw and Ropkins, 2012; R Core Team,  
480 2019). As an example, results from a very short event (13/07 h.16-18) singled out by the model and representing the  
481 highest sea salt contribution during summer are reported in Fig. S3 (Supplement). Before and during the event, south-  
482 western air masses ~~originated from south-west compatible with~~ coming from the Ligurian sea where observed while soon  
483 after the event, there was a rapid change of wind direction. These hours were characterised by an average hHigh wind  
484 speeds were recorded during the episode (of  $4.8 \pm 1.7$  m s<sup>-1</sup> (with a maximum peak of  $9.5$  m s<sup>-1</sup>) compared to  $1.9 \pm 1.0$   
485 m s<sup>-1</sup> average wind speed recorded during characterising the summer campaign.

486 When marine air masses are transported to polluted sites, sea salt particles ~~are characterised by~~ show a Cl deficit due to  
487 reactions with sulphuric and nitric acid (Seinfeld and Pandis, 2006) ~~and~~ In this case, the factor chemical profile ~~was is~~  
488 expected to be enriched in sulphate and nitrate. In this work, nitrate was not present in the aged sea salt chemical profile;  
489 a very rough estimate (Lee et al., 1999) gave a maximum expected contribution of 2 % (about 82 ng m<sup>-3</sup>) of the total  
490 nitrate mass in atmosphere; that can be considered negligible in terms of mass contribution of the sources.

491 Temporal patterns of Cl concentrations (not inserted in the multi-time resolution analysis as being a weak variable) during  
492 marine aerosol episodes were exploited to further confirm the factor-to-source association. ~~As an example, a very short~~  
493 ~~event (13/07 h.16-18) singled out by the model and representing the highest sea salt contribution during summer was~~  
494 ~~analysed in further detail. Before and during the sea salt event, air masses originated from south-west compatible with~~

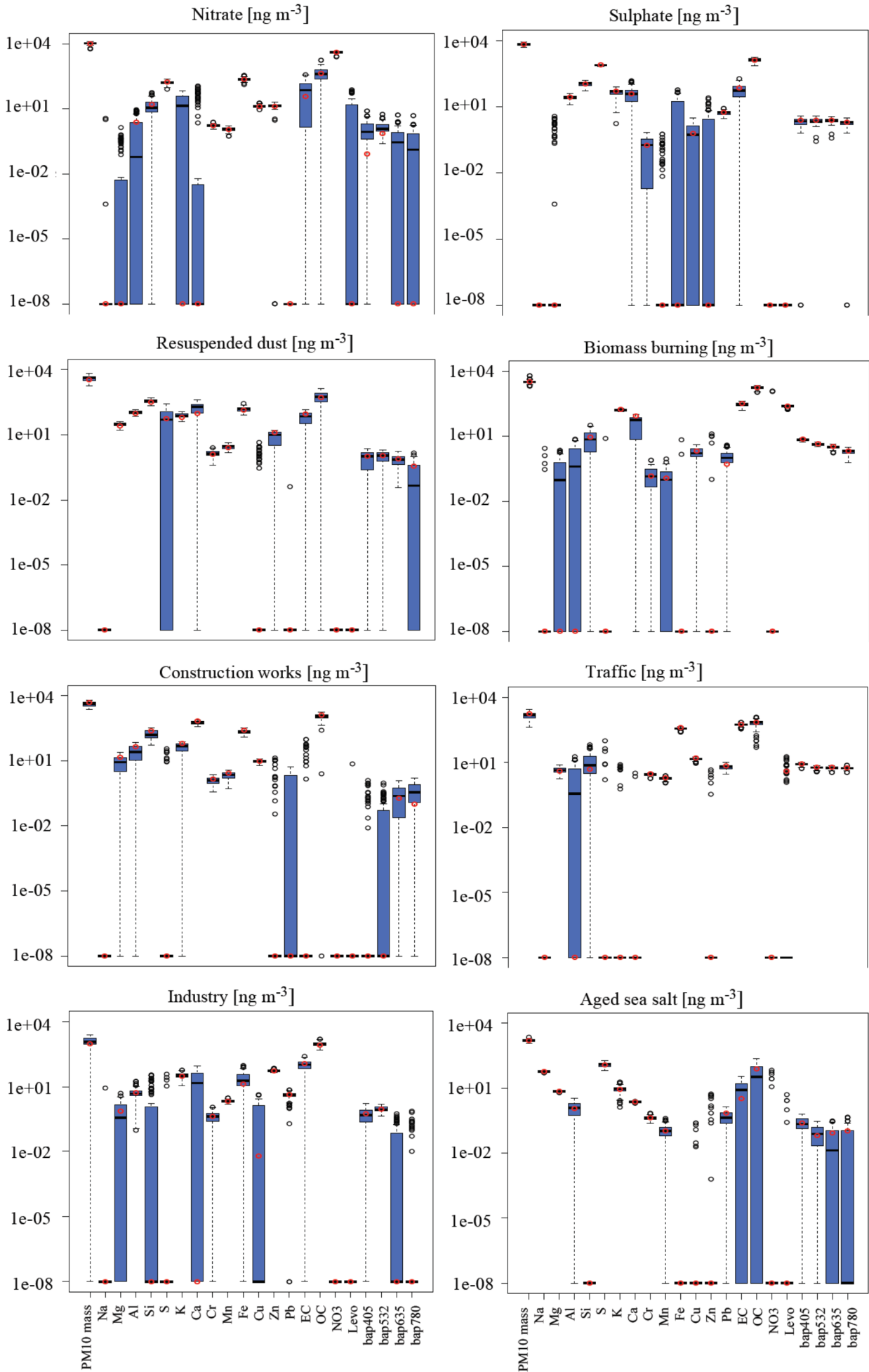
495 ~~Ligurian sea while soon after the event, there was a rapid change of wind direction (Fig. S3, in the Supplement). These~~  
 496 ~~hours were characterised by an average high wind speed of  $4.8 \pm 1.7 \text{ m s}^{-1}$  (with a maximum peak of  $9.5 \text{ m s}^{-1}$ ) compared~~  
 497 ~~to  $1.9 \pm 1.0 \text{ m s}^{-1}$  average wind speed recorded during the summer campaign. In addition, Cl concentration and aged sea~~  
 498 ~~salt pattern showed an evident temporal coincidence in peak occurrence during the short summer event (Fig. 4), thus~~  
 499 ~~supporting the source identification. Moreover, during this episode only the Cl coarse fraction increased (Fig. S4, in the~~  
 500 ~~Supplement) and reached about 90 % of total PM10 Cl concentration; Cl/Na ratio was  $0.38 \pm 0.05$ , consistent with an~~  
 501 ~~aging of marine air masses during advection showing the typical Cl depletion, due to the interaction between sea salt~~  
 502 ~~particles and polluted air masses (Seinfeld and Pandis, 2006).~~



503  
 504 Figure 4: Temporal patterns of aged sea salt source retrieved from the multi-time resolution model and Cl concentrations  
 505 measured in atmospheric aerosol.

506  
 507 Bootstrap analysis was performed to evaluate the uncertainties associated to source profiles (Crespi et al., 2016). 100 runs  
 508 were carried out (see Fig. 5, values expressed in  $\text{ng m}^{-3}$  or  $\text{Mm}^{-1}$  on a logarithmic scale); factors were well mapped, with  
 509 Pearson coefficients always higher than 0.97, and tracers for each source showed small interquartile range, supporting the  
 510 goodness of the solution presented in this work.





513

514 Figure 5: Box plot of the bootstrap analysis on the 8-factor constrained solution. The red dots represent the output values  
515 of the solution of the model; the black lines the medians from the bootstrap analysis; the blue bars the 25<sup>th</sup> and 75<sup>th</sup>  
516 percentile; the dotted lines the interval equal to 1.5 the interquartile range and the black dots the outliers from this interval.

517

### 518 *3.3 Improving source apportionment with optical tracers*

519 First of all, the use of the absorption coefficient determined at different wavelengths as input variable in the multi-time  
520 resolution model, strengthened the identification of the sources, suggesting that it can be exploited when specific chemical  
521 tracers are not available (e.g. levoglucosan for biomass burning). To prove that, a separate source apportionment study  
522 was performed with EPA PMF 5.0 (Norris et al., 2014), ~~introducing using~~ only hourly elemental concentrations from  
523 samples collected by the streaker sampler and hourly  $b_{ap}$  at different  $\lambda$  measured by PP\_UniMI on the same filters as input  
524 variables. Streaker samples typically lack of a complete chemical characterisation; in particular, important chemical  
525 tracers such as levoglucosan and EC are not available. In this analysis,  $b_{ap}$  assessed at different wavelengths resulted  
526 ~~particularly useful for the identification~~ effective in identifying of the biomass burning factor that explained a significant  
527 percentage of the  $b_{ap}$  itself (from 25 % to 35 % depending on  $\lambda$ ) (Fig. S5, in the Supplement); without ~~this additional~~  
528 ~~information~~ the optical variables, the factor-to-source assignment would be otherwise based only on the presence of  
529 elemental potassium although it is well-known that K cannot be considered an unambiguous tracer as it is emitted by a  
530 variety of sources (see for example Pachon et al., 2013; and references therein). Furthermore, results showed that the  
531 absorption coefficient contribution was higher than 45 % in the factor labelled as traffic, highlighting the importance of  
532 exhaust emissions in a factor that would be ~~otherwise differently~~ characterised ~~mainly on by~~ elements related to non-  
533 exhaust emissions (Cu, Fe, Cr).

534 From the multi-time resolution model, the two factors identified as biomass burning and traffic were the main contributors  
535 to aerosol absorption in atmosphere and showed significant EVF values. At 780 and 405 nm, traffic contributions  
536 ~~Contributions~~ to  $b_{ap}$  were 55 % and 42 %; biomass burning accounted for for traffic and 20 % and 36 % ~~for biomass~~  
537 ~~burning at 780 and 405 nm, respectively~~. The Explained Variation (EVF) of  $b_{ap}$  has the maximum value at 405 nm for  
538 biomass burning (0.32) and at 780 nm for traffic (0.49), showing the tendency to decrease and increase with the  
539 wavelength, respectively.

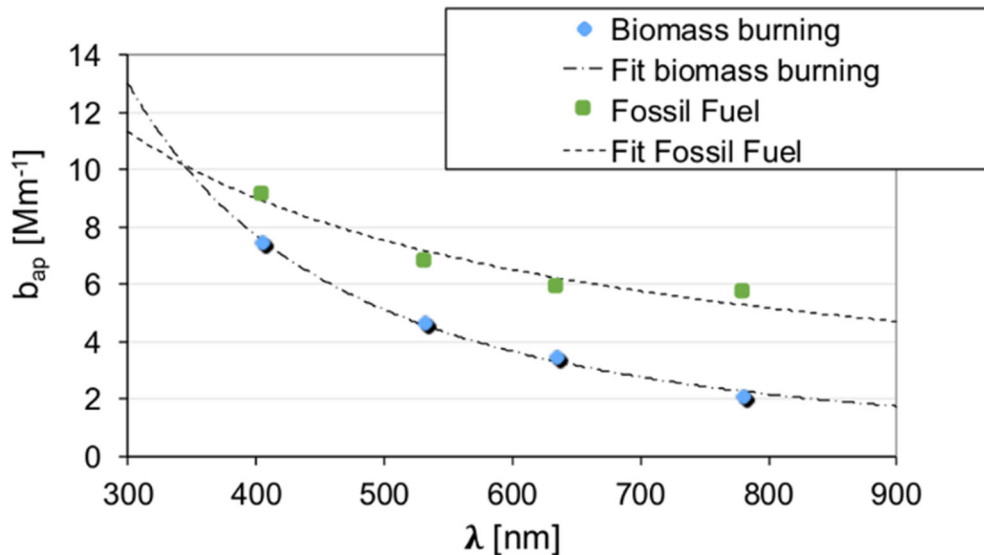
540 The third contributor to aerosol absorption in atmosphere was the sulphate factor, with a contribution comparable to the  
541 biomass burning one at 780 nm (about 20 % of the total reconstructed  $b_{ap}$  at this wavelength). The sulphate factor  
542 contained a small fraction of EC, as previously discussed (see Sect. 3.2). This might be explained considering that  
543 non/weakly light-absorbing material can form a coating able to enhance particle absorption (Bond and Bergstrom, 2006;

544 Fuller et al., 1999) within a few days after emission (~~Bond et al., 2006~~). Laboratory experiments and simulations from in-  
545 situ measurements highlighted absorption amplification for absorbing particles coated with secondary organic aerosol  
546 (Schnaiter et al., 2003; Moffet and Prather, 2009). ~~These processes related to P-particles aging can become important in is~~  
547 ~~a significant process in~~ the Po valley due to low atmospheric dispersion conditions and ~~they it~~ might explain the relatively  
548 high contribution of the sulphate factor to the absorption coefficient in respect to the other sources (~~excluding apart from~~  
549 traffic and biomass burning). ~~Among the other sources, R~~esuspended dust was the main contributor at all wavelengths  
550 (between 3 % and 7 % of the total reconstructed  $b_{ap}$ , depending on the wavelength), likely due to the role of iron minerals.  
551 The other ~~four~~ sources were less relevant in terms of EVF values and overall contributed for less than 11 %.

552 ~~It is noteworthy that opposite~~In contrast to the approach used in source apportionment ~~optical~~ models based on optical  
553 ~~measurements data~~, like the widespread Aethalometer model (Sandradewi et al., 2008a) and MWA model (Massabò et  
554 al., 2015; Bernardoni et al., 2017b), ~~it is noteworthy that~~ no a-priori information about  $\alpha$  values ~~the Absorption Ångström~~  
555 ~~Exponent ( $\alpha$ )~~ of the fossil fuel and biomass burning sources was introduced in the multi-time resolution model; ~~instead~~  
556 ~~and~~ an estimate for ~~the  $\alpha$  values~~ was directly retrieved from the model. ~~A further~~Another literature approach used Delta-  
557 C as an input variable together with chemical aerosol components in source apportionment models and was very effective  
558 in separating traffic (especially diesel) emissions from biomass combustion emissions (Wang et al., 2011, 2012). ~~It has to~~  
559 ~~be mentioned that optical models are typically based on a two-source hypothesis (i.e. biomass burning and fossil fuel~~  
560 ~~emissions); an exception reported in previous works (Wang et al., 2011) concerned the use of Delta-C used as an input~~  
561 ~~variable together with chemical aerosol components in source apportionment models and proved to be very effective in~~  
562 ~~separating traffic (especially diesel) emissions from biomass combustion emissions.~~

563 ~~Hereafter,~~ In order to compare ~~the~~ multi-time resolution model and ~~optical~~ models based on optical ~~measurements data~~  
564 ~~results~~, contributions due to traffic and industry (i.e. emissions most likely connected to fossil fuel usage) were added up  
565 and labelled as “fossil fuel emissions”. In accordance with the two-source approach used in the Aethalometer model, the  
566 discussion about optical properties will be hereafter focused on the biomass burning and fossil fuel sources considering  
567 that sulphate and resuspended dust factors were less significant also in terms of EVF for optical variables, ranging from  
568 0.08 to 0.12 and from 0.03 and 0.06, respectively, depending on the wavelength.

569 In Fig. 6 the wavelength dependence of  $b_{ap}$  for the biomass burning and the fossil fuel profiles obtained with the multi-  
570 time resolution model is shown; as  $\alpha$  values can show significant differences when calculated using different pairs of  $\lambda$   
571 (Sandradewi et al., 2008b), here we performed a fitting procedure considering  $b_{ap} \propto \lambda^{-\alpha}$ . Results were  $\alpha_{BB}$  ( $\alpha$  biomass  
572 burning) = 1.83 and  $\alpha_{FF}$  ( $\alpha$  fossil fuels) = 0.80; the range of variability of  $\alpha$  values was estimated with the bootstrap  
573 analysis obtaining 0.78-0.88 for  $\alpha_{FF}$  and 1.65-1.88 for  $\alpha_{BB}$  (as 25<sup>th</sup> and 75<sup>th</sup> percentile, respectively).



574

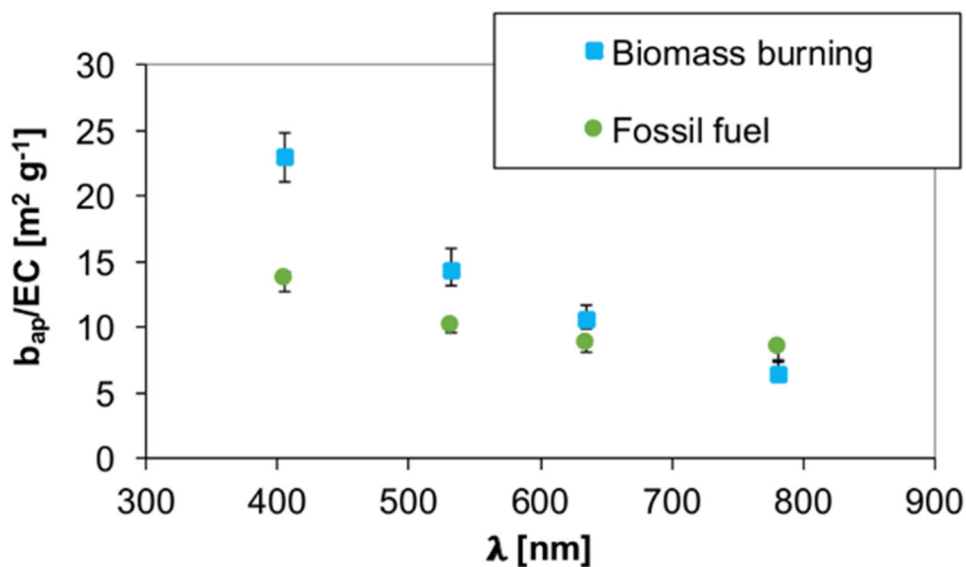
575 Figure 6:  $b_{ap}$  dependence on  $\lambda$  for biomass burning and fossil fuel emissions.

576

577 Zotter et al. (2017) reported a possible combination of  $\alpha_{FF}=0.8$  and  $\alpha_{BB}=1.8$  when EC concentration from fossil fuel  
 578 combustion (estimated with radiocarbon measurements) is between 40 % and 85 % of the total EC concentration; in this  
 579 work, the fraction of EC ascribed by the multi-time model to fossil fuel sources was 56 %. [The combination 0.9 and 1.68](#)  
 580 [for  \$\alpha\_{FF}\$  and  \$\alpha\_{BB}\$ , respectively, was also suggested when in the study there are no or only limited additional information](#)  
 581 [\(e.g. from <sup>14</sup>C measurements\). Therefore, from the wide range of possible combinations reported in the literature it is](#)  
 582 [clear that the assessment of  \$\alpha\_{BC}\$  \(assumed to be equal to  \$\alpha\_{FF}\$  in source apportionment optical models based on optical](#)  
 583 [measurements data\) is still an issue and both experimental and simulation studies are in progress to reduce uncertainties](#)  
 584 and give a better evaluation of this ~~relevant keyoptical~~ parameter.

585 The  $\alpha_{BB}$  value retrieved by the model was very similar to values reported by Zotter et al. (2017) and also comparable to  
 586 1.86 found for biomass burning by Sandradewi et al. (2008a) and 1.8 obtained by Massabò et al. (2015) who used also  
 587 independent <sup>14</sup>C measurements for checking. The  $\alpha_{FF}$  value resulted in the range 0.8-1.1 typically reported in ~~optical~~  
 588 source apportionment studies [based on optical measurements data](#) (e.g. Bernardoni et al., 2017b; Zotter et al., 2017; and  
 589 references therein). Indeed, the sampling site was an urban background station in Milan ~~where aerosol aging is a relevant~~  
 590 ~~process~~ and our samples ~~were~~ hardly ~~had been~~ impacted by fresh traffic emissions. Considering ~~this feature~~ [the aged nature](#)  
 591 of Milan aerosol, the average  $\alpha_{FF}$  was ~~included in the wide range of~~ [comparable to](#) estimates for BC coated particles  
 592 reported in [the literature works](#) (approx. 0.6-1.3, see e.g. Liu et al., 2018) and obtained by both ambient measurement  
 593 (e.g. Fischer and Smith, 2018; and references therein) and numerical simulations (e.g. Gyawali et al., 2009; Liu et al.  
 594 2018; and references therein).

595 Results here reported allow also to study the relationship between the absorption coefficient and the mass of black carbon  
 596 (BC), i.e. the so called Mass Absorption Cross section (~~MAC~~) at different wavelengths. The  $MAC(\lambda) = b_{ap}(\lambda)/BC$   
 597 relationship assumes that ~~black carbon (BC)~~ is the only light-absorbing species present; however, this assumption is not  
 598 always valid, since [the transport of mineral dust from desert areas](#) and brown carbon (~~BrC~~) can significantly contribute  
 599 to aerosol absorption. During our monitoring campaign, no ~~significant~~ contribution from [Saharan mineral](#) dust was  
 600 observed; opposite, biomass burning was ~~proved~~ proven to be ~~a relevant~~ an important source so that BrC was certainly a  
 601 significant contributor (Fuzzi et al., 2015) as also suggested by  $\alpha_{BB} = 1.83$  in the biomass burning factor. The possible  
 602 overestimation of BC when total  $b_{ap}$  is ascribed to BC only is usually minimised choosing a wavelength higher than 600  
 603 nm, exploiting the spectral dependence of absorption from different aerosol compounds (Petzold et al., 2013).  
 604 EC concentration retrieved from the chemical profiles (see Fig. 3) was used as a proxy for BC to estimate source-  
 605 dependent  $b_{ap}(\lambda)$ -to-BC ratio. Results are represented in Fig. 7. It is noteworthy that here this ratio is intentionally not  
 606 indicated as MAC, since overestimation of the BC absorption especially at lower  $\lambda$  might occur (see previous discussion).  
 607 BrC is expected to give a small contribution in the fossil fuel source; therefore, the best approximation for  $MAC(\lambda)$  values  
 608 are likely the  $b_{ap}(\lambda)$ -to-BC ratios observed in the fossil fuel source at our monitoring site. They resulted ~~to be~~  $13.7 \text{ m}^2 \text{ g}^{-1}$   
 609 ~~at for~~  $\lambda = 405 \text{ nm}$ ,  $10.2 \text{ m}^2 \text{ g}^{-1}$  ~~for~~  $\lambda = 532 \text{ nm}$ ,  $8.8 \text{ m}^2 \text{ g}^{-1}$  ~~at for~~  $\lambda = 635 \text{ nm}$ ,  $8.6 \text{ m}^2 \text{ g}^{-1}$  ~~at for~~  $\lambda = 780 \text{ nm}$ . ~~For~~  $\lambda =$   
 610  $550 \text{ nm}$  Bond and Bergstrom (2006) reported a MAC value of  $7.5 \pm 1.2 \text{ m}^2 \text{ g}^{-1}$  for uncoated fresh emitted particles and  
 611 MAC values in polluted regions ranging from 9 to  $12 \text{ m}^2 \text{ g}^{-1}$ , attributable to absorption enhancement due to particles  
 612 coating. The MAC estimate obtained in this work from multi-time resolution model ~~for~~  $532 \text{ nm}$  is comparable to  
 613 literature values ~~above reported thus confirming~~ and it confirms the importance of aging processes in atmosphere on the  
 614 optical properties of particles.



615

616 Figure 7:  $b_{ap}$ -to-EC ratio dependence on  $\lambda$  for biomass burning and fossil fuel emissions. Error bars represent the 25<sup>th</sup> and  
 617 75<sup>th</sup> percentile retrieved from the bootstrap analysis.

618

619 Ratios represented in Fig. 7 are less comparable at  $\lambda=405$  nm (see also Table S4, in the Supplement) due to the significant  
 620 contribution of BrC to  $b_{ap}$  at this wavelength in the biomass burning factor.

621 No seasonal differences in the atmospheric ratios were observed but at  $\lambda = 405$  nm (see Table S4, in the Supplement), for  
 622 which winter values ~~are were~~ higher than summer ones ( $17.8 \pm 0.4$  and  $14.2 \pm 0.5$ , respectively); ~~this result can be~~  
 623 ~~explained considering due to~~ the influence of biomass burning emissions on BrC concentration in atmosphere during the  
 624 ~~winter cold~~ season.

625 From the outputs of the modelling approach here proposed, the apportionment of the biomass burning and fossil fuel  
 626 contributions to  $b_{ap}$  at different wavelengths was also obtained. As expected, the relative contribution to the total  
 627 reconstructed  $b_{ap}$  ascribed to the biomass burning factor ~~decreases-decreased~~ with increasing  $\lambda$ , opposite to the  
 628 contribution from fossil fuel combustion which ~~gives-gave~~ the highest contribution at 780 nm (Table 2); in addition, the  
 629 latter contribution ~~prevails-prevailed~~ at all wavelengths at the investigated site.

	$\lambda = 405$ nm	$\lambda = 532$ nm	$\lambda = 635$ nm	$\lambda = 780$ nm
<b>Biomass burning</b>	36 % (31 %-36 %)	29 % (25 %-30 %)	26 % (23 %-27 %)	20 % (16 %-22 %)
<b>Fossil fuels</b>	45 % (41 %-46 %)	43 % (39 %-44 %)	45 % (41 %-47 %)	55 % (48 %-55 %)

Table 2: Average contribution to total reconstructed  $b_{ap}$  for the biomass burning and fossil fuel factors; in parenthesis 25<sup>th</sup>  
 and 75<sup>th</sup> percentile are reported.

630

#### 631 4. Conclusions

632 The multi-time resolution model implemented through [the](#) Multilinear Engine (ME-2) script allowed the analysis of  
 633 experimental data collected at different time scales, coupling the detailed chemical speciation at low time resolution and  
 634 the temporal information given by high time resolution samples. The effect of the introduction of the aerosol absorption  
 635 coefficient ( $b_{ap}$ ) measured at different wavelengths in the modelling process was investigated and gave promising results.  
 636 First of all, a more robust identification of sources was provided; secondly, it paved the way to the retrieval of optical  
 637 apportionment and optical characterisation of the sources (e.g. estimate of source-specific Absorption Ångström Exponent  
 638 -  $\alpha$  - and [Mass Absorption Cross section – MAC-](#) at different wavelengths). It is worthy to note that ~~at the state of the~~  
 639 ~~art-currently~~ in source apportionment ~~optical~~ models [based on optical measurements data](#) (e.g. Aethalometer model)

640 values for  $\alpha$  related to fossil fuel emissions and biomass burning are fixed by the modeller thus carrying a large part of  
641 the uncertainties in the model results. Considering that the estimates for the Absorption Ångström Exponent were here  
642 obtained as a result of a quite complex modelling approach (i.e. using multi-time resolution datasets ~~collected on limited~~  
643 ~~periods joining chemical and optical variables~~) and without any a-priori assumption, the results obtained ~~—although~~  
644 ~~obviously affected by a certain degree of uncertainty due to both experimental data and modelling process (here estimated~~  
645 ~~while typically not taken into consideration for fixed  $\alpha$  values used in the literature)~~—were fairly comparable to literature  
646 results and gave a further tool ~~aimed at assessing to assess~~ more robust source-related  $\alpha$  values. Obviously these estimates  
647 are affected by a certain degree of uncertainty due to both experimental data and modelling process (while uncertainties  
648 are typically not taken into consideration for fixed  $\alpha$  values used in the literature). In perspective, joining together different  
649 approaches such as the receptor modelling here proposed and e.g.  $^{14}\text{C}$  ~~measurements data~~ and artefact-free  $b_{\text{ap}}$   
650 measurements will lead to better estimates of the Absorption Ångström Exponent; ~~work is in progress at our laboratories~~  
651 ~~to achieve this goal.~~

652 The original approach described in this work can be applied to ~~any~~ source apportionment ~~study studies~~ using any suitable  
653 dataset (not necessarily with multi-time resolution). Besides the traditional source apportionment, the impact of different  
654 sources on the aerosol absorption coefficient was estimated; this piece of information can be very useful to formulate  
655 strategies of pollutants abatement, in order to improve air quality and to face climate challenges. In particular, at the  
656 investigated site secondary compounds constituted the highest contribution in terms of PM10 mass (52 % on average),  
657 while the two factors identified as biomass burning and traffic were found to be the most significant contributors to aerosol  
658 light absorption in atmosphere, in agreement with available literature ~~works~~.

659

## 660 Acknowledgements

661 This work was partially funded by the Italian National Institute of Nuclear Physics under ~~the~~ INFN experiments  
662 (DEPOTMASS and TRACCIA) and by ACTRIS-IT ~~funded the publication of the paper~~. The authors thank Prof. Paola  
663 Fermo (Dept. of Chemistry, University of Milan) for availability of the Sunset instrument to perform EC/OC analyses  
664 and ARPA – Lombardia for meteorological data availability. The mechanical workshop of the Dept. of Physics –  
665 University of Milan is gratefully acknowledged for the realisation of parts of the polar photometer. The authors are  
666 grateful to Prof. Philip Hopke for hints on multi-time resolution ME-2.

667

## 668 Data availability.

669 The data in the study are available from the authors upon request (roberta.vecchi@unimi.it).

670 **Supplement.**

671 The supplement related to this article is available online.

672

673 **Author contributions.**

674 ACF performed streaker sampling and related optical analysis, implemented the advanced model, analysed the results,  
675 and drafted the paper. GV contributed to model implementation, data reduction and Hysplit back-trajectories retrieval.  
676 VB, SV, and REP carried out the sampling campaign on filters, performed the optical measurements and data analysis.  
677 GC, SN, and FL performed PIXE analysis and data reduction. DM and PP carried out ionic characterisation on filters and  
678 data analysis. RV was responsible for the design and coordination of the study, the synthesis of the results and the final  
679 version of the paper. All authors contributed to the interpretation of the results obtained with the new approach here  
680 described and revised the manuscript content giving a final approval of the version to be submitted. RV and ACF reviewed  
681 the paper addressing reviewers' comments.

682

683 **Competing interests.**

684 The authors declare that they have no conflict of interest.

685

686 **References**

687 Amato F., Alastuey A., Karanasiou A., Lucarelli F., Nava S., Calzolari G., Severi M., Becagli S., Gianelle V.N., Colombi  
688 C., Alves C., Custódio D., Nunes T., Cerqueira M., Pio C., Eleftheriadis K., Diapouli E., Reche C., Minguillón M.C.,  
689 Manousakas M.I., Maggos T., Vratolis S., Harrison R.M. and Querol X.: AIRUSE-LIFE+: a harmonized PM speciation  
690 and source apportionment in five southern European cities, *Atmos. Chem. Phys.*, 16, 3289-3309,  
691 <https://doi.org/10.5194/acp-16-3289-2016>, 2016.

692 Andreae M.O. and Gelencsér A.: Black carbon or brown carbon? The nature of light-absorbing carbonaceous aerosols,  
693 *Atmos. Chem. Phys.*, 6, 3131-3148, <https://doi.org/10.5194/acp-6-3131-2006>, 2006.

694 Belis C.A., Larsen B.R., Amato F., El Haddad I., Favez O., Harrison R.M., Hopke P.K., Nava S., Paatero P., Prévot A.,  
695 Quass U., Vecchi R. and Viana M.: European Guide on Air Pollution Source Identification with Receptor Models,  
696 Luxembourg: Publications Office of the European Union, Joint Research Center – Institute for Environment and  
697 Sustainability, European Union, <https://doi.org/10.2788/9332>, 2014.

698 Belis C.A., Karagulian F., Amato F., Almeida M., Artaxo P., Beddows D.C.S., Bernardoni V., Bove M.C., Carbone S.,  
699 Cesari D., Contini D., Cuccia E., Diapouli E., Eleftheriadis K., Favez O., El Haddad I., Harrison R.M., Hellebust S.,  
700 Hovorka J., Jang E., Jorquera H., Kammermeier T., Karl M., Lucarelli F., Mooibroek D., Nava S., Nøjgaard J.K., Paatero

701 P., Pandolfi M., Perrone M.G., Petit J.E., Pietrodangelo A., Pokorná P., Prati P., Prevot A.S.H., Quass U., Querol X.,  
702 Saraga D., Sciare J., Sfetsos A., Valli G., Vecchi R., Vestenius M., Yubero E. and Hopke P.K.: A new methodology to  
703 assess the performance and uncertainty of source apportionment models II: The results of two European intercomparison  
704 exercises, *Atmos. Environ.*, 123, 240-250, <https://doi.org/10.1016/j.atmosenv.2015.10.068>, 2015.

705 Bernardoni V., Vecchi R., Valli G., Piazzalunga A. and Fermo P.: PM<sub>10</sub> source apportionment in Milan (Italy) using  
706 time-resolved data, *Sci. Total Environ.*, 409, 4788-4795, <https://doi.org/10.1016/j.scitotenv.2011.07.048>, 2011.

707 Bernardoni V., Elser M., Valli G., Valentini S., Bigi A., Fermo P., Piazzalunga A. and Vecchi R.: Size-segregated  
708 aerosol in a hot-spot pollution urban area: Chemical composition and three-way source apportionment, *Environ. Pollut.*,  
709 231, 601-611, <https://doi.org/10.1016/j.envpol.2017.08.040>, 2017a.

710 Bernardoni V., Pileci R.E., Caponi L. and Massabò D.: The Multi-Wavelength Absorption Analyzer (MWAA) model as  
711 a tool for source and component apportionment based on aerosol absorption properties: application to samples collected  
712 in different environments, *Atmosphere*, 8, 218, <https://doi.org/10.3390/atmos8110218>, 2017b.

713 Bernardoni V., Valli G. and Vecchi R.: Set-up of a multi-wavelength polar photometer for the off-line measurement of  
714 light absorption properties of atmospheric aerosol collected with high-temporal resolution, *J. Aerosol. Sci.*, 107, 84-93,  
715 <https://doi.org/10.1016/j.jaerosci.2017.02.009>, 2017c.

716 Bigi A. and Ghermandi G.: Long-term trend and variability of atmospheric PM<sub>10</sub> concentration in the Po Valley, *Atmos.*  
717 *Chem. Phys.*, 14, 4895-4907, <https://doi.org/10.5194/acp-14-4895-2014>, 2014.

718 Bond T.C. and Bergstrom R.W.: Light absorption by carbonaceous particles: an investigative review, *Aerosol Sci. Tech.*,  
719 40, 27-67, <https://doi.org/10.1080/02786820500421521>, 2006.

720 Bond T.C., Doherty S.J., Fahey D.W., Forster P.M., Berntsen T., DeAngelo B.J., Flanner M.G., Ghan S., Kärcher B.,  
721 Koch D., Kinne S., Kondo Y., Quinn P.K., Sarofim M.C., Schultz M.G., Schulz M., Venkataraman C., Zhang H., Zhang  
722 S., Bellouin N., Guttikunda S.K., Hopke P.K., Jacobson M.Z., Kaiser J.W., Klimont Z., Lohmann U., Schwarz J.P.,  
723 Shindell D., Storelvmo T., Warren S.G. and Zender C.S.: Bounding the role of black carbon in the climate system: A  
724 scientific assessment, *J. Geophys. Res.-Atmos.*, 118, 5380-5552, <https://doi.org/10.1002/jgrd.50171>, 2013.

725 Brown S.G., Eberly S., Paatero P. and Norris G.A.: Methods for estimating uncertainty in PMF solutions: Examples with  
726 ambient air and water quality data and guidance on reporting PMF results, *Sci. Total Environ.*, 518-519, 626-635,  
727 <https://doi.org/10.1016/j.scitotenv.2015.01.022>, 2015.

728 Calzolari G., Chiari M., Lucarelli F., Mazzei F., Nava S., Prati P., Valli G. and Vecchi R.: PIXE and XRF analysis of  
729 particulate matter samples: an inter-laboratory comparison, *Nucl. Instrum. Meth. B*, 266, 2401-2404,  
730 <https://doi.org/10.1016/j.nimb.2008.03.056>, 2008.

731 Calzolari G., Lucarelli F., Chiari M., Nava S., Giannoni M., Carraresi L., Prati P. and Vecchi R.: Improvements in PIXE

732 analysis of hourly particulate matter samples, *Nucl. Instrum. Meth. B*, 363, 99-104,  
733 <https://doi.org/10.1016/j.nimb.2015.08.022>, 2015.

734 Cappa C.D., Lack D.A., Burkholder J.B., and Ravishankara A.R.: Bias in filter-based aerosol light absorption  
735 measurements due to organic aerosol loading: Evidence from laboratory measurements. *Aerosol Sci. Tech.*, 42, 1022-  
736 1032, <https://doi.org/10.1080/02786820802389285>, 2008.

737 Carslaw D.C. and Ropkins K.: Openair — an R package for air quality data analysis. *Environ. Modell. Softw.* 27/28,  
738 52-61, <https://doi.org/10.1016/j.envsoft.2011.09.008>, 2012

739 Crespi A., Bernardoni V., Calzolari G., Lucarelli F., Nava S., Valli G. and Vecchi R.: Implementing constrained multi-  
740 time approach with bootstrap analysis in ME-2: an application to PM<sub>2.5</sub> data from Florence (Italy), *Sci. Total Environ.*,  
741 541, 502-511, <https://doi.org/10.1016/j.scitotenv.2015.08.159>, 2016.

742 Crilley L.R., Lucarelli F., Bloss W.J., Harrison R.M., Beddows D.C., Calzolari G., Nava S., Valli G., Bernardoni V. and  
743 Vecchi R.: Source Apportionment of Fine and Coarse Particles at a Roadside and Urban Background Site in London  
744 during the Summer ClearLo Campaign, *Environ. Pollut.*, 220, 766-778, <https://doi.org/10.1016/j.envpol.2016.06.002>,  
745 2017.

746 D'Alessandro A., Lucarelli F., Mandò P.A., Marcazzan G., Nava S., Prati P., Valli G., Vecchi R. and Zucchiatti A.:  
747 Hourly elemental composition and sources identification of fine and coarse PM<sub>10</sub> particulate matter in four Italian towns,  
748 *J. Aerosol Sci.*, 34, 243-259, [https://doi.org/10.1016/S0021-8502\(02\)00172-6](https://doi.org/10.1016/S0021-8502(02)00172-6), 2003.

749 Dall'Osto, M., Querol, X., Amato, F., Karanasiou, A., Lucarelli, F., Nava, S., Calzolari, G. and Chiari, M.: Hourly  
750 elemental concentrations in PM<sub>2.5</sub> aerosols sampled simultaneously at urban background and road site during SAPUSS  
751 e diurnal variations and PMF receptor modelling, *Atmos. Chem. Phys.*, 13, 4375-4392, <https://doi.org/10.5194/acp-13-4375-2013>, 2013.

752

753 Davies N.W., Fox C., Szpek K., Cotterell M.I., Taylor J.W., Allan J.D., Williams P.I., Trembath J., Haywood J.M., and  
754 Langridge J.M.: Evaluating biases in filter-based aerosol absorption measurements using photoacoustic spectroscopy,  
755 *Aerosol Meas. Tech.*, 12, 3417–3434, <https://doi.org/10.5194/amt-12-3417-2019>, 2019.

756 Draxler R.R. and Hess G.D.: An overview of the HYSPLIT\_4 modelling system for trajectories, dispersion, and  
757 deposition, *Aust. Meteorol. Mag.*, 47, 295-308, 1998.

758 Fialho P., Hansen A.D.A. and Honrath R.E.: Absorption coefficients by aerosols in remote areas: a new approach to  
759 decouple dust and black carbon absorption coefficients using seven-wavelength Aethalometer data, *J. Aerosol Sci.*, 36,  
760 267-282, <https://doi.org/10.1016/j.jaerosci.2004.09.004>, 2005.

761 Fischer D.A. and Smith G.D.: A portable, four wavelength, single-cell photoacoustic spectrometer for ambient aerosol  
762 absorption, *Aerosol Sci. Tech.*, 52, 393-406, <https://doi.org/10.1080/02786826.2017.1413231>, 2018.

763 Fuller K.A., Malm W.C. and Kreidenweis S.M.: Effects of mixing on extinction by carbonaceous particles, *J. Geophys.*  
764 *Res.*, 104, 15941-15954, <https://doi.org/10.1029/1998JD100069>, 1999.

765 Fuzzi S., Baltensperger U., Carslaw K., Decesari S., Denier van der Gon H., Facchini M.C., Fowler D., Koren I., Langford  
766 B., Lohmann U., Nemitz E., Pandis S., Riipinen I., Rudich Y., Schaap M., Slowik J.G., Spracklen D.V., Vignati E., Wild  
767 M., Williams M. and Gilardoni S.: Particulate matter, air quality and climate: lessons learned and future needs, *Atmos.*  
768 *Chem. Phys.*, 15, 8217-8299, <https://doi.org/10.5194/acp-15-8217-2015>, 2015.

769 Gyawali M., Arnott W.P., Lewis K. and Moosmüller H.: In situ aerosol optics in Reno, NV, USA during and after the  
770 summer 2008 California wildfires and the influence of absorbing and non-absorbing organic coatings on spectral light  
771 absorption, *Atmos.Chem.Phys.*, 9, 8007-8015, <https://doi.org/10.5194/acp-9-8007-2009>, 2009.

772 Hennigan C.J., Sullivan A.P., Collett J.L.Jr and Robinson A.L.: Levoglucosan stability in biomass burning particles  
773 exposed to hydroxyl radicals, *Geophys. Res. Lett.*, 37, 9, <https://doi.org/10.1029/2010GL043088>, 2010.

774 Henry R.C.: History and fundamentals of multivariate air quality receptor models, *Chemometr. Intell. Lab.*, 37, 37-42,  
775 [https://doi.org/10.1016/S0169-7439\(96\)00048-2](https://doi.org/10.1016/S0169-7439(96)00048-2), 1997.

776 Hopke P.K.: Review of receptor modeling methods for source apportionment, *J. Air Waste Manage.*, 66, 3, 237-259,  
777 <https://doi.org/10.1080/10962247.2016.1140693>, 2016.

778 INEMAR - ARPA Lombardia: INEMAR, Inventario Emissioni in Atmosfera: emissioni in Regione Lombardia nell'anno  
779 2014 - dati finali, ARPA Lombardia Settore Monitoraggi Ambientali,  
780 <http://www.inemar.eu/xwiki/bin/view/Inemar/HomeLombardia>, 2018.

781 IPCC: Climate Change 2013: The Physical Science Basis. Contribution of Working Group I to the Fifth Assessment  
782 Report of the Intergovernmental Panel on Climate Changes, Stocker T.F., Qin D., Plattner G.-K., Tignor M., Allen S.K.,  
783 Boschung J., Nauels A., Xia Y., Bex V. and P.M. Midgley, Cambridge University Press, Cambridge, United Kingdom  
784 and New York, NY, USA, <https://doi.org/10.1017/CBO9781107415324>, 2013.

785 Kim E., Hopke P.K. and Edgerton E.S.: Source identification of Atlanta aerosol by positive matrix factorization, *J. Air*  
786 *Waste Manage.*, 53, 6, 731-739, <https://doi.org/10.1080/10473289.2003.10466209>, 2003.

787 Kuo C.-P., Liao H.-T., Chou C.C.-K. and Wu C.-F.: Source apportionment of particulate matter and selected volatile  
788 organic compounds with multiple time resolution data, *Sci. Total Environ.*, 472, 880-887,  
789 <https://doi.org/10.1016/j.scitotenv.2013.11.114>, 2014.

790 Lack D.A., Cappa C.D., Covert D.S., Baynard T., Massoli P., Sierau B., Bates T.S., Quinn P.K., Lovejoy E.R., and  
791 Ravishankara A.R.: Bias in filter-based aerosol light absorption measurements due to organic aerosol loading: Evidence  
792 from ambient measurements. *Aerosol Sci. Tech.*, 42, 1033-1041, <https://doi.org/10.1080/02786820802389277>, 2008.

793 Lee E., Chan C.K. and Paatero P.: Application of positive matrix factorization in source apportionment of particulate

794 pollutants in Hong Kong, *Atmos. Environ.*, 33, 3201-3212, [https://doi.org/10.1016/S1352-2310\(99\)00113-2](https://doi.org/10.1016/S1352-2310(99)00113-2), 1999.

795 Liao H.-T., Chou C.C.-K., Chow J.C., Watson J.G., Hopke P.K. and Wu C.-F.: Source and risk apportionment of selected  
796 VOCs and PM<sub>2.5</sub> species using partially constrained receptor models with multiple time resolution data, *Environ. Pollut.*,  
797 205, 121-130, <https://doi.org/10.1016/j.envpol.2015.05.035>, 2015.

798 Liu C., Chung C.E., Yin Y. and Schnaiter M.: The absorption Ångström exponent of black carbon: from numerical  
799 aspects. *Atmos. Chem. Phys.*, 18, 6259-6273, <https://doi.org/10.5194/acp-2017-836>, 2018.

800 Marcazzan G.M., Vaccaro S., Valli G. and Vecchi R.: Characterisation of PM<sub>10</sub> and PM<sub>2.5</sub> particulate matter in the  
801 ambient air of Milan (Italy), *Atmos. Environ.*, 35, 4639-4650, [https://doi.org/10.1016/S1352-2310\(01\)00124-8](https://doi.org/10.1016/S1352-2310(01)00124-8), 2001.

802 Marcazzan G.M., Ceriani M., Valli G. and Vecchi R.: Source apportionment of PM<sub>10</sub> and PM<sub>2.5</sub> in Milan (Italy) using  
803 receptor modelling, *Sci. Total Environ.*, 317, 137-147, [https://doi.org/10.1016/S0048-9697\(03\)00368-1](https://doi.org/10.1016/S0048-9697(03)00368-1), 2003.

804 Mason B.: Principles of geochemistry, 3<sup>rd</sup> Edition, John Wiley & Sons, New York, 1966.

805 Massabò D., Caponi L., Bernardoni V., Bove M.C., Brotto P., Calzolari G., Cassola F., Chiari M., Fedi M.E., Fermo P.,  
806 Giannoni M., Lucarelli F., Nava S., Piazzalunga A., Valli G., Vecchi R. and Prati P.: Multi-wavelength optical  
807 determination of black and brown carbon in atmospheric aerosols, *Atmos. Environ.*, 108, 1-12,  
808 <https://doi.org/10.1016/j.atmosenv.2015.02.058>, 2015.

809 Massabò D., Caponi L., Bove M.C. and Prati P.: Brown carbon and thermal-optical analysis: A correction based on optical  
810 multi-wavelength apportionment of atmospheric aerosols, *Atmos. Environ.*, 125, 119-125,  
811 <https://doi.org/10.1016/j.atmosenv.2015.11.011>, 2016.

812 Moffet R.C. and Prather K.A.: In-situ measurements of the mixing state and optical properties of soot with implications  
813 for radiative forcing estimates, *Proc. Natl. Acad. Sci. USA*, 106, 11872-11877, <https://doi.org/10.1073/pnas.0900040106>,  
814 2009.

815 Norris G., Duvall R., Brown S. and Bai S.: EPA Positive Matrix Factorization (PMF) 5.0. Fundamentals and User Guide,  
816 U.S. Environmental Protection Agency, Washington, DC, 2014.

817 Ogulei D., Hopke P.K., Zhou L., Paatero P., Park S.S. and Ondov J.M.: Receptor modeling for multiple time resolved  
818 species: the Baltimore supersite, *Atmos. Environ.*, 39, 3751-3762, <https://doi.org/10.1016/j.atmosenv.2005.03.012>, 2005.

819 Paatero P.: Least squares formulation of robust non-negative factor analysis, *Chemometr. Intell. Lab.*, 37, 23-35,  
820 [https://doi.org/10.1016/S0169-7439\(96\)00044-5](https://doi.org/10.1016/S0169-7439(96)00044-5), 1997.

821 Paatero P.: The Multilinear Engine – A Table-drive least squares program for solving multilinear problems, including the  
822 n-way parallel factor analysis model, *J. Comput. Graph. Stat.*, 8, 4, 854-888,  
823 <https://doi.org/10.1080/10618600.1999.10474853>, 1999.

824 Paatero P.: User's guide for the Multilinear Engine program "ME2" for fitting multilinear and quasi-multilinear models,

825 University of Helsinki, Department of Physics, Finland, 2000.

826 Paatero P.: User's Guide for Positive Matrix Factorization programs PMF2 and PMF3, Part 2: reference, available  
827 [www.helsinki.fi/~paatero/PMF/pmf2.zip](http://www.helsinki.fi/~paatero/PMF/pmf2.zip) (PMFDOC2.pdf), last update 2010.

828 Paatero P.: The Multilinear Engine (ME-2) script language (v. 1.352), available with the program ME-2 (me2scrip.txt).  
829 2012.

830 Paatero P.: User's guide for positive matrix factorization programs PMF2 and PMF3, part 1: Tutorial, available at  
831 [www.helsinki.fi/~paatero/PMF/pmf2.zip](http://www.helsinki.fi/~paatero/PMF/pmf2.zip) (PMFDOC1.pdf), last update 2015.

832 Paatero P.: Interactive comment on a paper submitted to ACPD, available at <https://doi.org/10.5194/acp-2018-784-RC2>,  
833 2018

834 Paatero P. and Hopke P.K.: Rotational tools for factor analytic models. *J. Chemometr.*, 23, 91-100,  
835 <https://doi.org/10.1002/cem.1197>, 2009.

836 Paatero P. and Tapper U.: Positive Matrix Factorization: a non-negative factor model with optimal utilization of error  
837 estimates of data values, *Environmetrics*, 5, 111-126, <https://doi.org/10.1002/env.3170050203>, 1994.

838 Pachon J.E., Weber R.J., Zhang X., Mulholland J.A. and Russell A.G.: Revising the use of potassium (K) in the source  
839 apportionment of PM<sub>2.5</sub>, *Atmos. Pollut. Res.*, 4, 14-21, <https://doi.org/10.5094/APR.2013.002>, 2013.

840 Peré-Trepat E., Kim E., Paatero P. and Hopke P.K.: Source apportionment of time and size resolved ambient particulate  
841 matter measured with a rotating DRUM impactor, *Atmos. Environ.*, 41, 5921-5933,  
842 <https://doi.org/10.1016/j.atmosenv.2007.03.022>, 2007.

843 Perrino C., Catrambone M., Dalla Torre S., Rantica E., Sargolini T. and Canepari S.: Seasonal variations in the chemical  
844 composition of particulate matter: a case study in the Po Valley. Part I: macro-components and mass closure, *Environ.*  
845 *Sci. Pollut. Res.*, 21, 3999-4009, <https://doi.org/10.1007/s11356-013-2067-1>, 2014.

846 Perrone M.G., Larsen B.R., Ferrero L., Sangiorgi G., De Gennaro G., Udisti R., Zangrando R., Gambaro A. and  
847 Bolzacchini E.: Sources of high PM<sub>2.5</sub> concentrations in Milan, Northern Italy: Molecular marker data and CMB  
848 modelling. *Sci. Total Environ.*, 414, 343-355, <https://doi.org/10.1016/j.scitotenv.2011.11.026>, 2012.

849 Petzold A., Ogre J.A., Fiebig M., Laj P., Li S.-M., Baltensperger U., Holzer-Popp T., Kinne S., Pappalardo G., Sugimoto  
850 N., Wehrli C., Wiedensohler A. and Zhang X.-Y.: Recommendations for the interpretation of "black carbon"  
851 measurements, *Atmos. Chem. Phys.*, 13, 8365-8379, <https://doi.org/10.5194/acp-13-8365-2013>, 2013.

852 Piazzalunga A., Fermo P., Bernardoni V., Vecchi R., Valli G. and De Gregorio M.A.: A simplified method for  
853 levoglucosan quantification in wintertime atmospheric particulate matter by high performance anion-exchange  
854 chromatography coupled with pulsed amperometric detection, *Int. J. Environ. Anal. Chem.*, 90, 934-947,  
855 <https://doi.org/10.1080/03067310903023619>, 2010.

856 Piazzalunga A., Bernardoni V., Fermo P., Valli G. and Vecchi R. Technical note: On the effect of water-soluble  
857 compounds removal on EC quantification by TOT analysis in urban aerosol samples, *Atmos. Chem. Phys.*, 11, 10193–  
858 10203, <https://doi.org/10.5194/acp-11-10193-2011>, 2011.

859 Piazzalunga A., Bernardoni V., Fermo P. and Vecchi R.: Optimisation of analytical procedures for the quantification of  
860 ionic and carbonaceous fractions in the atmospheric aerosol and application to ambient samples, *Anal. Bioanal. Chem.*,  
861 405, 1123-1132, <https://doi.org/10.1007/s00216-012-6433-5>, 2013.

862 Polissar A., Hopke P.K., Paatero P., Malm W.C. and Sisler J.F.: Atmospheric aerosol over Alaska: elemental composition  
863 and sources. *J. Geophys. Res.* 103, 19045-19057, <https://doi.org/10.1029/98JD01212>, 1998.

864 Pope III C.A. and Dockery D.W.: Health effects of fine particulate air pollution: lines that connect, *J. Air Waste Manage.*,  
865 56, 709-742, <https://doi.org/10.1080/10473289.2006.10464485>, 2006.

866 [R Core Team: R: A language and environment for statistical computing. R Foundation for Statistical Computing, Vienna,  
867 Austria, <http://www.R-project.org>, 2019.](http://www.R-project.org)

868 Robinson A.L., Donahue N.M. and Rogge W.F.: Photochemical oxidation and changes in molecular composition of  
869 organic aerosol in the regional context, *J. Geophys. Res.*, 111, D3, <https://doi.org/10.1029/2005JD006265>, 2006.

870 Rolph G., Stein A. and Stunder B.: Real-time Environmental Application and Display sYstem: READY, *Environ. Modell.*  
871 *Softw.*, 95, 210-228, <https://doi.org/10.1016/j.envsoft.2017.06.025>, 2017.

872 Sandradewi J., Prévôt A.S.H., Szidat S., Perron N., Alfarra M.R., Lanz V.A., Weingartner E. and Baltersperger U.:  
873 Using aerosol light absorption measurements for the quantitative determination of wood burning and traffic emission  
874 contributions to particulate matter, *Environ. Sci. Technol.*, 42, 3316-3323, <https://doi.org/10.1021/es702253m>, 2008a.

875 Sandradewi J., Prévôt A.S.H., Weingartner E., Schmidhauser R., Gysel M., and Baltersperger U.: A study of wood  
876 burning and traffic aerosols in an Alpine valley using a multi-wavelength Aethalometer, *Atmos. Environ.*, 2, 101–112,  
877 [doi:10.1016/j.atmosenv.2007.09.034](https://doi.org/10.1016/j.atmosenv.2007.09.034), 2008b.

878 Schnaiter M., Horvath H., Möhler O., Naumann K.-H., Saathoff H. and Schöck O.W.: UV-VIS-NIR spectral optical  
879 properties of soot and soot-containing aerosols, *J. Aerosol Sci.*, 34, 1421-1444, [https://doi.org/10.1016/S0021-  
8502\(03\)00361-6](https://doi.org/10.1016/S0021-<br/>880 8502(03)00361-6), 2003.

881 Seinfeld J.H. and Pandis S.N.: Atmospheric chemistry and physics: from air pollution to climate change, 2<sup>nd</sup> edition, John  
882 Wiley & Sons, INC, Hoboken, New Jersey, 2006.

883 Simoneit B.R.: Levoglucosan, a tracer for cellulose in biomass burning atmospheric particles. *Atmos. Environ.*, 33, 173-  
884 182, [https://doi.org/10.1016/S1352-2310\(98\)00145-9](https://doi.org/10.1016/S1352-2310(98)00145-9), 1999.

885 Sofowote U.M., Healy R.M., Su Y., Deboz J., Noble M., Munoz A., Jeong C.-H., Wang J.M., Hilker N., Evans G.J. and  
886 Hopke P.K.: Understanding the PM<sub>2.5</sub> imbalance between a far and near-road location: Results of high temporal frequency

887 source apportionment and parameterization of black carbon, *Atmos. Environ.*, 173, 277-288,  
888 <https://doi.org/10.1016/j.atmosenv.2017.10.063>, 2018.

889 Stein A.F., Draxler R.R., Rolph G.D., Stunder B.J.B., Cohen M.D. and Ngan F.: NOAA's Hysplit atmospheric transport  
890 and dispersion modeling system, *Bull. Am. Meteorol. Soc.*, 96, 2059-2077, [https://doi.org/10.1175/BAMS-D-14-](https://doi.org/10.1175/BAMS-D-14-00110.1)  
891 00110.1, 2015.

892 Thorpe A. and Harrison R.M.: Sources and properties of non-exhaust particulate matter from road traffic: A review, *Sci.*  
893 *Total Environ.*, 400, 270-282, <https://doi.org/10.1016/j.scitotenv.2008.06.007>, 2008.

894 ~~Valentini S., Weber P., Bernardoni V., Bundke U., Massabò D., Petzold A., Prati P., Valli G. and Vecchi R.: Multi-~~  
895 ~~Wavelength Measurement of Aerosol Optical Properties: Laboratory Intercomparison of In Situ and Filter Based~~  
896 ~~Techniques, in Abstracts Book 12th International Conference on Carbonaceous Particles in the Atmosphere (ICCPA)~~  
897 ~~2019, 149, <https://iccpa2019.univie.ac.at/abstracts/>, 2019.~~

898 Vecchi R., Marcazzan G., Valli G., Ceriani M. and Antoniazzi C.: The role of atmospheric dispersion in the seasonal  
899 variation of PM1 and PM2.5 concentration and composition in the urban area of Milan (Italy), *Atmos. Environ.*, 38, 4437-  
900 4446, <https://doi.org/10.1016/j.atmosenv.2004.05.029>, 2004.

901 Vecchi R., Marcazzan G. and Valli G.: A study on nighttime-daytime PM10 concentration and elemental composition in  
902 relation to atmospheric dispersion in the urban area of Milan (Italy), *Atmos. Environ.*, 41, 2136-2144,  
903 <https://doi.org/10.1016/j.atmosenv.2006.10.069>, 2007.

904 Vecchi R., Bernardoni V., Fermo P., Lucarelli F., Mazzei F., Nava S., Prati P., Piazzalunga A. and Valli G.: 4-hours  
905 resolution data to study PM10 in a "hot spot" area in Europe, *Environ. Monit. Assess.*, 154, 283-300,  
906 <https://doi.org/10.1007/s10661-008-0396-1>, 2009.

907 Vecchi R., Bernardoni V., Paganelli C. and Valli G.: A filter-based light absorption measurement with polar photometer:  
908 effects of sampling artefacts from organic carbon, *J. Aerosol. Sci.*, 70, 15-25,  
909 <https://doi.org/10.1016/j.jaerosci.2013.12.012>, 2014.

910 Vecchi R., Bernardoni V., Valentini S., Piazzalunga A., Fermo P. and Valli G.: Assessment of light extinction at a  
911 European polluted urban area during wintertime: Impact of PM1 composition and sources, *Environ. Pollut.*, 233, 679-  
912 689, <https://doi.org/10.1016/j.envpol.2017.10.059>, 2018.

913 Vecchi R., Piziali F.A., Valli G., Favaron M. and Bernardoni V.: Radon-based estimates of equivalent mixing layer  
914 heights: A long-term assessment, *Atmos. Environ.*, 197, 150-158, <https://doi.org/10.1016/j.atmosenv.2018.10.020>, 2019.

915 Viana M., Kuhlbusch T.A.J., Querol X., Alastuey A., Harrison R.M., Hopke P.K., Winiwarter W., Vallius M., Szidat S.,  
916 Prévôt A.S.H., Hueglin C., Bloemen H., Wählin P., Vecchi R., Miranda A.I., Kasper-Giebl A., Maenhaut W. and  
917 Hitzenberger R.: Source apportionment of particulate matter in Europe: A review of methods and results, *J. Aerosol Sci.*,

918 39, 827-849, <https://doi.org/10.1016/j.jaerosci.2008.05.007>, 2008.

919 Wang Y., Hopke P.K., Rattigan O.V., Xia X., Chalupa D.C. and Utell M.J.: Characterization of residential wood  
920 combustion particles using the two-wavelength aethalometer, *Environ. Sci. Technol.*, 45, 7387-7393,  
921 <https://doi.org/10.1021/es2013984>, 2011.

922 Wang Y., Hopke P.K., Rattigan O.V., Chalupa D.C. and Utell M.J.: Multiple-year black carbon measurements and source  
923 apportionment using Delta-C in Rochester, New York, *J. Air Waste Manage.*, 62, 8, 880-887,  
924 <https://doi.org/10.1080/10962247.2012.671792>, 2012.

925 Watson J.G.: Visibility: Science and Regulation, *J. Air Waste Manage.*, 52, 628-713,  
926 <https://doi.org/10.1080/10473289.2002.10470813>, 2002.

927 Xie M., Chen X., Holder A.L., Hays M.D., Lewandowski M., Offenberg J.H., Kleindienst T.E., Jaoui M. and Hannigan  
928 M.P.: Light absorption of organic carbon and its sources at a southeastern U.S. location in summer, *Environ. Pollut.*, 244,  
929 38-46, <https://doi.org/10.1016/j.envpol.2018.09.125>, 2019.

930 Yang M., Howell S.G., Zhuang J. and Huebert B.J.: Attribution of aerosol light absorption to black carbon, brown carbon,  
931 and dust in China – interpretations of atmospheric measurements during EAST-AIRE, *Atmos. Chem. Phys.*, 9, 2035-  
932 2050, <https://doi.org/10.5194/acp-9-2035-2009>, 2009.

933 Zhou L., Hopke P.K., Paatero P., Ondov J.M., Pancras J.P., Pekney N.J. and Davidson C.I.: Advanced factor analysis for  
934 multiple time resolution aerosol composition data, *Atmos. Environ.*, 38, 4909-4920,  
935 <https://doi.org/10.1016/j.atmosenv.2004.05.040>, 2004.

936 Zotter P., Herich H., Gysel M., El-Haddad I., Zhang Y., Mocnik G., Hüglin C., Baltensperger U., Szidat S. and Prévôt  
937 A.S.H.: Evaluation of the absorption Ångström exponents for traffic and wood burning in the Aethalometer-based source  
938 apportionment using radiocarbon measurements of ambient aerosol, *Atmos. Chem. Phys.*, 17, 4229-4249,  
939 <https://doi.org/10.5194/acp-17-4229-2017>, 2017.

940

941

942

943

944

945

946

947

948 **List of Captions**

949 Figure 1: Diurnal profile of Fe and Cu concentrations (in  $\text{ng m}^{-3}$ ).

950 Figure 2: [Diurnal profile of aerosol absorption coefficient \(in  \$\text{Mm}^{-1}\$ \) measured at different wavelengths.](#)

951 [Diurnal profile of the aerosol absorption coefficient measured at different wavelengths in  \$\text{Mm}^{-1}\$ .](#)

952 [Figure 3: \(a\) Chemical profiles of the 8-factor constrained solution ; \(b\)  \$b\_{\text{ap}}\$  apportionment of the 8-factor constrained](#)

953 [solution. The blue bars represent the chemical profile \(output of the matrix F normalised on mass\), the green bars the](#)

954 [output values of the matrix F for the optical variables, and the black dots the EVF.](#)

955 ~~Figure 3: (a) Chemical profiles of the 8-factor constrained solution (b)  $b_{\text{ap}}$  apportionment of the 8-factor constrained~~

956 ~~solution. The blue bars represent the chemical profile (output of the matrix F normalised on mass), the green bars the~~

957 ~~output values of the matrix F, and the black dots the EVF.~~

958 Figure 4: Temporal patterns of aged sea salt source retrieved from the multi-time resolution model and Cl concentrations

959 measured in atmospheric aerosol.

960 Figure 5: Box plot of the bootstrap analysis on the 8-factor constrained solution. The red dots represent the output values

961 of the solution of the model; the black lines the medians from the bootstrap analysis; the blue bars the 25<sup>th</sup> and 75<sup>th</sup>

962 percentile; the dotted lines the interval equal to 1.5 the interquartile range and the black dots the outliers from this interval.

963 Figure 6:  $b_{\text{ap}}$  dependence on  $\lambda$  for biomass burning and fossil fuel emissions.

964 Figure 7:  $b_{\text{ap}}$ -to-EC ratio dependence on  $\lambda$  for biomass burning and fossil fuel emissions. Error bars represent the 25<sup>th</sup> and

965 75<sup>th</sup> percentile retrieved from the bootstrap analysis.

966

967 Table 1: Absolute and relative average source contributions to PM10 mass in the 8-factor constrained solution.

968 Table 2: Average contribution to total reconstructed  $b_{\text{ap}}$  for the biomass burning and fossil fuel factors; in parenthesis 25<sup>th</sup>

969 and 75<sup>th</sup> percentile are reported.

970